NASA Technical Memorandum 81158

Analysis of the Performance of the Drive System and Diffuser of the Langley Unitary Plan Wind Tunnel

Lowell E. Hasel and Robert L. Stallings, Jr.

October 1980

NASA

NASA Technical Memorandum 83168

Analysis of the Performance of the Drive System and Diffuser of the Langley Unitary Plan Wind Tunnel

Lowell E. Hasel and Robert L. Stallings, Jr.
Langley Research Center
Hampton, Virginia

National Aeronautics
and Space Administration

Scientific and Technical
Information Branch

1981

SUMMARY

A broad program to reduce the energy consumption of the Unitary Plan Wind Tunnel was initiated in 1973. As a part of this program, a study was made to determine if potential methods for increasing the operating efficiencies of the tunnel could be formulated. The study was conducted by determining the performance characteristics of the drive system components and then analyzing the overall performance of the wind-tunnel system.

With the current (1977-1981) operating procedures, the power input to the test-section airflow is from 50 to 85 percent of the power input to the drive system. A major portion of the excess power is absorbed by the drive system compressors which are operating in a bypass mode to match the test-section airflow requirements in the Mach number range from 1.46 to 2.00. By late 1981, mechanical and control system improvements should allow the bypassing compressors to be operated at lower pressures if no adverse effects on main drive vibrations occur. This improvement could reduce the average energy requirements of the tunnel by as much as 10 percent. Additional small reductions in energy may be attainable by optimizing the compressor inlet guide-vane positions for both normal and bypass operation.

The operating-pressure-ratio characteristics of the tunnel are high relative to what should be attainable with an efficient variable-geometry diffuser system. These high pressure ratios are forced on the system by the airflow-matching characteristics of the test section and compressor system. Consequently, there is very little justification for attempting to improve the performance of the existing diffuser system.

INTRODUCTION

The necessity since 1973 to minimize the use of energy in the United States has resulted in a number of studies at the Langley Research Center to determine methods for achieving this goal. These studies have included a reexamination of the operation of research facilities which use large amounts of energy. One such facility is the Unitary Plan Wind Tunnel (UPWT). Figure 1 summarizes the electrical energy used by the UPWT for the fiscal years of 1966-1980. Kilowatt hours (kWh) used per tunnel operating hour, kWh used per fiscal year, and the percentage of total Langley Research Center electrical energy used by the UPWT are plotted as a function of fiscal year. From 1975 to 1980, the tunnel used an average of about 23 million kWh per year (1 kWh = 3.6 MJ). This amount corresponds to about 16 percent of the total usage by Langley.

From 1974 through 1980, the unit cost of the electrical energy used by the major wind-tunnel facilities at Langley increased at a rapid rate, reaching a level of $0.0538 per kWh in fiscal year 1980 (fig. 2). The total cost in 1980 of the energy for the UPWT was $1.215 million (fig. 2). It should be noted that the unit power costs include a demand charge which is a fixed amount, independent of the total consumption for the year. The total facility power usage was below average in 1975 and 1977. Hence, the unit costs for these 2 years were unusually high, as can be noted by the deviations from the trend in figure 2. As a matter of general interest, the operating hours per year for the UPWT are shown in figure 3. From 1977 through 1980, the tunnel averaged about 900 hours of operation per year.

Since 1973 a number of approaches have been adopted to reduce the UPWT energy consumption. These approaches include minimization of the length of the test programs, reduction of both the test Reynolds number and test-section stagnation temperature, installation of new tunnel equipment and data acquisition systems, and improved operational procedures. The energy savings which have resulted cannot be accurately judged from the energy consumed per operating hour (fig. 1) because the yearly variations in the program test requirements, such as Mach number and Reynolds number, affect the overall energy requirements.

Early in 1977, a decision was made to reexamine the performance characteristics of the UPWT. The objective was to determine if potential methods for increasing the operating efficiencies of the drive and diffuser systems could be formulated. A thorough search of tunnel run logs and records was made, but none of the performance data taken when the tunnel was placed in operation in 1956 could be found. The only data uncovered were from a 1966 limited study of the performance of two of the UPWT compressors. These data were inadequate for the purposes of the proposed study. It was, therefore, necessary to obtain a new set of performance data before the desired analysis could be completed.

The objective of this report is to document the measured performance characteristics of the UPWT at Mach numbers from 1.50 to 4.60 and the analysis which has been made of these results. The performance characteristics, including the energy requirements of each of the compressors and the combined system, are presented as functions of test-section Mach number and compressor-inlet corrected mass flow. The performance of the supersonic-subsonic, variable-geometry diffuser system is also discussed along with the associated airflow-matching characteristics of the test-section diffuser and the compressor drive system. Finally, on the basis of the above analyses, comments are made regarding the potential for reducing the energy requirements of the tunnel.

Use of trade names or manufacturers' names does not constitute an official endorsement of such products or manufacturers, either expressed or implied, by NASA.

SYMBOLS

A	cross-sectional area, m^2
A_f	effective aerodynamic flow cross-sectional area, m^2
A_g	geometric cross-sectional area, m^2
A^*	sonic flow area, m^2
CR	compression ratio, $p_{t,d}/p_{t,i}$
c_p	specific heat of air at constant pressure, J/kg-K
K	constant in equation for calculating duct total pressure loss
M	Mach number
N_{Re}	Reynolds number, per meter
P	power, MW

p	static pressure, kPa
p_t	stagnation pressure, kPa
$p_{t,NS}$	stagnation pressure behind normal shock, kPa
Δp_t	total pressure loss in ducting downstream of compressor discharge, kPa
q	dynamic pressure, kPa
R	gas constant (for air, $R = 287.05$ J/kg-K)
rpm	revolutions per minute
T	static temperature, K
TS	test section
ΔT_t	temperature rise through compressor, $T_{t,d} - T_{t,i}$, K
UPWT	Unitary Plan Wind Tunnel
V	velocity, m/sec
w	mass flow, kg/sec
$\frac{w\sqrt{\theta}}{\delta}$	mass flow corrected to standard conditions, kg/sec
γ	specific heat ratio (for air, $\gamma = 1.4$)
δ	corrected pressure, $P_t/101.32$ kPa
δ^*	boundary-layer displacement thickness, cm
η	compressor adiabatic efficiency, percent
θ	corrected temperature, $T_t/288.2$ K
ρ	density, kg/m^3
ϕ	supersonic diffuser contraction ratio, A_{TS}/A_{SM}

Subscripts:

av	average
D	duct
d	compressor discharge
E	compressor E
i	inlet
max	maximum

meas	measured
SM	second minimum
TS	test section
t	stagnation
1	first stage
2	second stage
3	third stage
4	fourth stage

DESCRIPTION OF TUNNEL

The Langley Unitary Plan Wind Tunnel is a closed-circuit, variable-pressure facility with two variable Mach number test sections which are approximately 1.22 m in height and width and 2.13 m in length. The Mach number ranges of the two test sections are 1.46 to 2.80 and 2.30 to 4.63. An exterior view of the facility is shown in figure 4. Figure 5 presents a schematic drawing of the primary components of the tunnel.

Reference 1 contains a detailed description of the various components of the tunnel, which is not repeated herein. The description and operation of the tunnel drive system and the supersonic-subsonic diffuser system are reviewed below because the performance of these two components is the main subject of the data analysis.

The drive system (fig. 5) consists of six centrifugal compressors identified by the letters I, C, D, E, F, and G. Power is supplied by a 47.2-MW (63 333-hp) synchronous motor and a 14.9-MW (20 000-hp) variable-speed motor which is also used as a starting motor. The combined overload one-half-hour rating of the two motors is 74.6 MW (100 000 hp). The six compressors and the synchronous motor are connected by one continuous shaft. This system has an overall length of about 36.58 m. Power from the variable-speed motor is transferred into the main drive shaft through a speed-increasing gear box. A photograph of the drive system is shown in figure 6. Compressor G is located at the right edge of the picture. The variable-speed motor is near the left edge. The compressors are standard commercial designs with the following ratings:

Characteristic	Compressor		
	C, D, E	I, F	G
Design inlet volume flow, m^3/min	8438	4219	1699
Design inlet corrected mass flow, kg/sec	163	81.6	32.8
Design inlet temperature, K	322	322	322
Design pressure ratio.....	1.95	1.95	2.24
Design efficiency, percent	73	73	80
Design rpm	3600	3600	3600
Maximum inlet absolute pressure, kPa	276	207(I) 310(F)	462
Stages	1	1	3
Variable inlet guide vanes	Yes	Yes	First stage only
Manufacturer	Roots-Connersville Blower Corp.	Roots-Connersville Blower Corp.	Clark Bros. Co., Inc.

The compression ratio required to operate the tunnel varies from about 1.5 to 18 as the Mach number increases from 1.46 to 4.63. At the lower Mach numbers, one stage of compression is sufficient to provide the required pressure ratio, but three compressors operating in parallel (I, C, and D) are required to match the test-section mass flow. As Mach number increases, second, third, and fourth stages of compression are added to provide the necessary operating pressure ratios. At Mach numbers of 3.96 and higher, only two first-stage compressors, C and D, are required to match the test-section mass flow. The following table summarizes the compressor operating sequences:

Operating mode	Test section	Mach number (nominal)	Stage of compression					
			Compressor					
			I	C	D	E	F	G
1-IA	1	1.46 to 2.16	1	1	1			
1-II	1	2.36 to 2.80	1	1	1	2		
2-II	2	2.30 to 2.98	1	1	1	2		
2-III	2	3.00 to 3.72	1	1	1	2	3	
2-IV	2	3.96 to 4.63		1	1	2	3	4

The flow paths through the tunnel piping for the various operating modes are shown by arrows and shading in figure 7. Remotely operated valves control these flow paths. Aftercoolers are provided for each compressor. Note that a precooler is installed ahead of the first stage.

The six compressors always operate at 3600 rpm and always remain connected to the common drive shaft even though one or more of the units are not being used to

provide the operating pressure ratios. Each of the unused compressors operates in a bypass mode. Valves are used to provide an isolated, closed-loop airflow circuit for each bypassing compressor. These isolated flow circuits are necessary to allow the compressors to operate in a normal, unstalled manner. When the tunnel was first placed in operation, the discharge pressure of each bypassing compressor was maintained at a subatmospheric level to minimize the power required by these units. However, it was soon noted that the main drive periodically had severe vibration problems, and that these vibrations could be reduced by loading the bypassing compressors (increasing the stagnation pressures).

At the time of the present study, the discharge loops of E, F, and G were always vented to atmospheric pressure when operating on bypass. The discharge loop of I was always vented to the discharge ducting of C and D. Note in the previous table that C and D never operate in the bypass mode.

As previously noted, all the compressors have remotely controlled, variable-position inlet guide vanes. These vanes are kept in the 100-percent-open position when processing the test-section airflow and in a 40-percent-open position during the bypass mode of operation.

The plan-view geometries of the two supersonic-subsonic, variable-geometry, remotely controlled diffuser systems are shown in figure 8. The height of each section is 1.22 m. The diffusers of test sections 1 and 2 can be contracted to geometric flow areas of 0.557 m^2 and 0.372 m^2, respectively. Based on a 1.22-m square test section, the corresponding maximum contraction ratios of the diffusers are 2.67 and 4.0, respectively. The operating contraction ratios vary with test-section Mach number.

DATA ACQUISITION AND REDUCTION

General

The performance characteristics of the UPWT drive system were determined by measuring the inlet and discharge static pressures and total temperatures of each compressor, the electrical energy input to the drive system, and the associated test-section conditions. These data were then reduced to the desired form for analysis. The details of the entire acquisition and reduction process are discussed in the remainder of this section.

Data Acquisition

Test-section conditions.- All the data were obtained at a test-section Reynolds number of 4.92×10^6 per meter. This Reynolds number, although lower than the nominal operating Reynolds number of 6.56×10^6, was selected to permit a single range of pressure instrumentation to be used through the test range of Mach numbers. The stagnation temperature was 338.9 K for Mach numbers from 1.50 to 3.70 and 352.8 K for Mach numbers from 3.85 to 4.60. The stagnation pressures varied from 39.98 kPa to 187.1 kPa as the Mach number increased from 1.50 to 4.60. The test-section stagnation pressures are given as a function of Mach number in table I.

Compressors.- The inlet and discharge static pressures and total temperatures were recorded from instrumentation installed during construction of the tunnel to measure compressor performance during acceptance tests. Typical installations of the

instrumentation are shown in figure 9. Generally, the data presented in the report were obtained by averaging four individual readings. Some of the pressure data were obtained from a manifold tube connected to the four static orifices. The averaged static pressure data for the bypassing compressors are presented in table II. The measured pressure data for the compressors processing the test-section mass flow were corrected to stagnation conditions, and these corrected values are presented in table I. The method of correction is described in a following section. All the averaged temperature data are presented in table III. Since the averaged pressure and temperature data for compressors C and D were essentially the same, the measurements for D are not presented.

Drive motors.- The energy input into the main drive motor system was generally read from two meters located on the tunnel control panel. These meters were small, and the reading accuracy was about ±1.0 MW. More accurate meters (±0.1 MW) were installed on the motors for the tests conducted to determine the energy consumed by the bypassing compressors.

Data Reduction

Compressor mass flow.- The compressor mass flow (in kilograms per second) was determined by calculating the flow through the test section using the following equation:

$$w_{TS} = \left[\frac{40.41 p_t A_f}{(A/A^*)\sqrt{T_t}}\right]_{TS}$$

This equation is derived in the appendix. The constant 40.41 has units of $kg\text{-}K^{1/2}/N\text{-}sec$. The calculations are based on the test-section effective aerodynamic flow area. This effective area consists of the geometric area (1.486 m^2 and 1.579 m^2 for test sections 1 and 2, respectively) minus a correction for the test-section boundary-layer displacement thickness. Presented in figure 10 is the variation of effective area with Mach number as determined from the measured displacement thickness shown in figure 11.

It should be noted that the geometric area of 1.579 m^2 for test section 2 is slightly in error. On the basis of data presented in reference 1, this value is too small by amounts varying from 1.9 percent at $M = 2.30$ to 1.5 percent at $M = 4.60$. The error is partially due to the fact that the geometric area of test section 2 changes slightly with Mach number. This condition does not exist in test section 1. Errors of this small magnitude have no impact on the significance of the data and have, therefore, not been corrected.

The absolute test-section mass flow quantities are plotted as a function of Mach number in figure 12 for the stagnation pressure conditions listed in table I. These mass flows decrease with Mach number, even though the stagnation pressure is increasing, because of the decreasing size of the nozzle throat. The slight discontinuity of the curves at $M = 3.8$ is due to the increase in stagnation temperature at which the tunnel is normally operated at the higher speeds.

For all operating modes except 2-IV, the first stage of compression is accomplished by compressors C, D, and I (fig. 7) operating in parallel. The mass flow split between the three compressors was not measured. The design mass flow of C and D is supposedly twice the mass flow of I. However, the analysis of the measured data from compressors E (identical to C and D) and F (identical to I) indicated that at a given pressure ratio the mass flow through I was about 0.69 of the mass flow through C or D. The first-stage mass flow split was, therefore, assumed to be

C	37 percent
D	37 percent
I	26 percent

During mode 2-IV operation, compressor I operates in the bypass mode, and the first-stage mass flow was assumed to be equally divided between compressors C and D.

Compressor stagnation pressures.- As previously mentioned, only static pressures were measured at the inlets and exits of the various compressors. For the compressors which were processing the test-section airflow, these static pressures could be corrected to the stagnation pressures because the compressor mass flows were known. These corrections were made by use of the following modified form of the basic mass flow equation derived in the appendix. The units of the constant 40.41 are $kg\text{-}K^{1/2}/N\text{-}sec$.

$$\frac{40.41 A_q p}{\sqrt{T_t} w} = \frac{p}{p_t} \frac{A_q}{A^*}$$

The quantities on the left side of the equation are all known, and those on the right side are a function only of the local duct Mach number. Figure 13 shows this relationship. Obviously, if the duct Mach number can be determined, the static pressures can be corrected to total values assuming that uniform flow exists across the duct and the effects of the boundary-layer displacement thickness are negligible. As a matter of general interest, the local duct Mach numbers varied from about 0.05 to 0.31. The highest Mach numbers occurred in the discharge duct of compressor G. The duct areas used in the above equation were measured at each pressure measurement location and are as follows:

Compressor	Duct area, m^2	
	Inlet side	Discharge side
I	2.61	1.14
C, D	3.54	1.56
E	3.56	1.56
F	2.58	1.15
G	.92	.30

Compressor power.- The power, in megawatts, which each compressor delivered to the tunnel airflow was calculated from the following equation:

$$P = 10^{-6} w_i c_p \Delta T$$

$$= 10^{-6} w_i c_p \left(T_{t,d} - T_{t,i}\right)_{meas}$$

Compressor efficiency.- The compressor efficiency η was defined as follows:

$$\eta = \frac{\text{Ideal power input}}{\text{Measured power input}} \times 100$$

$$= \frac{\Delta T_{t,ideal}}{\Delta T_{t,meas}} \times 100$$

$$= \frac{T_{t,i}\left[\left(\frac{p_{t,d}}{p_{t,i}}\right)_{meas}^{0.286} - 1\right]}{\left(T_{t,d} - T_{t,i}\right)_{meas}} \times 100$$

PRESENTATION AND DISCUSSION OF RESULTS

Drive System and Performance

Individual compressor performance.- The measured and calculated data for compressors I, C, E, F, and G are plotted in figure 14. No data are presented for compressor D since its measured performance was essentially the same as that of C. The corrected mass flow, compression ratio, temperature rise across the compressor, efficiency, and calculated power input to the airstream are plotted as a function of the test-section Mach number. The mass flows are presented in a standard form (corrected mass flow), which is often used for presenting compressor performance. In this form, the inlet mass flow is independent of its absolute pressure and temperature levels. The elongated diamond symbols denote data for bypass operating conditions. As previously mentioned, mass flow through the bypassing compressors was not measured. Lack of this information prohibited the direct calculation of the power input to the bypass airstreams.

The basic data as presented in figure 14 give a general picture of how each compressor operates over the entire Mach number range. As discussed later, at each Mach number the operating conditions of each compressor are established by its interaction with the other compressors processing the test-section mass flow, by the quantity of the test-section mass flow, and by the performance of the supersonic-subsonic diffuser system. This process is generally identified as the mass-flow-matching process which automatically occurs between the test-section diffuser system and the

compressor system. The discontinuities in operating conditions which occur at the mode changes are caused by these matching requirements. These discontinuities are most noticeable in the compression ratio and efficiency parameters.

It is interesting to note in figure 14 that the temperature rise across each compressor processing the test-section mass flow is relatively constant over the Mach number range, even though some of the compression ratios vary by large amounts. When the compression ratios are low, the efficiencies are also low, thus keeping the temperature rise high. Since the temperature-rise values are relatively constant, the calculated power requirements are primarily a function of the absolute test-section mass flow and, therefore, decrease as the Mach number increases. The corrected mass flow of compressor C is higher during mode 2-IV operation than during mode 2-III operation because compressor I, one of the first-stage compressors, has been shifted to the bypass operating mode.

The bypassing compressors operate with the inlet guide vanes at a 40-percent-open, instead of a 100-percent-open, position. Hence, the performance characteristics would be expected to be different. The magnitude of change of these characteristics varies by significant amounts among the compressors. The reasons for these differences are not known.

The compression ratio and efficiency characteristics of compressors E, F, and G are plotted in figure 15 as a function of the inlet corrected mass flow. As previously mentioned, when compressors E, F, and G are required in the system, each of these compressors processes all the test-section mass flow. The guide vanes were in the 100-percent-open position for all these data. The plus symbols mark the design point for each compressor. For compressors E and F, the data obtained from the various operating modes are in good agreement. Compressor G appears to be operating in a choked mode except for the 2.19 pressure ratio point (M_{TS} = 4.60). According to the manufacturer's specifications, compressors E and F should have identical performances except that the corrected mass flow of E should be twice that of F. Both the compressors exceeded the design pressure ratio of 1.95. Compressor F appears to have a peak compression ratio which is somewhat higher than that of E. The efficiencies both reach the design value of 0.73 but not necessarily at the design point. The mass flow capacities of E and F do not appear to be different by a factor of 2. The dashed curves in figure 15 were obtained by duplicating the shape of the compressor E curves by reducing by 31 percent the compressor E mass flow values at given levels of compression ratio and efficiency. The good agreement between the dashed curves and the compressor F data indicates that the corrected mass flow capacity of the F machine is about 69 percent of the E machine. It was on the basis of this plot that the mass flow through compressors I, C, and D was assumed to be 25 percent, 37 percent, and 37 percent, respectively, of the test-section mass flow whenever the three machines were operating in parallel.

Using the above assumed mass flow proportions, the measured performance of compressors I and C is shown in figure 16 as a function of the inlet corrected mass flow. The long-dashed curves in figure 16 are the faired data for compressors F and E from figure 15. Compressors C and E, and I and F are two sets of identical machines. Hence, one would expect the data presented in figures 15 and 16 to be in good agreement. The data in figure 16 verify that the agreement is good, although it appears that the average mass flow agreement would have been better if the assumed mass flow for compressor I had been 25 percent of the total first-stage mass flow.

It should be mentioned that the range of measured mass flow data for each compressor presented in figures 15 and 16 does not define the lower stable (stall-free) operating limit of any of the compressors. These data merely represent the operating ranges as determined by the match points of the test-section and compressor system mass flows. It appears from the shapes of the curves that the maximum flow values are fairly well defined, but there is no indication of what the minimum values for stable flow might be.

The measured performances of compressors C, E, and G are compared with the manufacturers' specification performances in figure 17. The plus symbols indicate the design points. The original specification plots show performance curves for several inlet guide-vane positions, but the specific guide-vane position for each curve was not given by the manufacturers. It appears that the specification mass flow characteristics differ significantly from the measured results. If the specification curves indicate the correct trends, the minimum stable values may be significantly less than those indicated by the data in figures 15 and 16.

In the mid-1960's, a brief unpublished study was made of the effects of the inlet guide-vane position on the performance of compressor F during mode 2-III operation. The guide-vane positions were varied from 100 to 60 percent of the fully open position. The data were obtained at stagnation pressures which varied from 110.3 kPa to 172.4 kPa and at a stagnation temperature of 338.9 K. Compression ratio, temperature-rise, and efficiency parameters from these tests are plotted as a function of the corrected mass flow in figure 18. This set of data is faired with short-dashed lines. The solid line is the fairing of the data presented in figure 15. The two sets of data for the 100-percent-open guide-vane position are in fairly good agreement. Varying the guide-vane position has a relatively small effect on compression ratio in comparison with what might have been expected from the undefined specification data shown for compressor E in figure 17(a). The effect becomes smaller as the mass flow decreases. Only small effects are indicated in efficiency and temperature-rise parameters. Reducing the guide-vane position from the 100-percent-open to the 60-percent-open setting reduces the temperature rise across the compressor by about 10 percent.

Overall drive-system performance. - The incremental and overall compression-ratio performance of the compressor system is shown in figure 19. Inlet total pressures to each stage of compression and the test-section total pressures, all referenced to the first-stage inlet total pressure, are plotted as a function of Mach number. Mode 1-II data have been omitted from this plot to simplify the data presentation. With the exception of the second stage of compression for mode 2-III (Mach numbers from 3.0 to 3.70), only the pressure ratio of the last stage of compression varies significantly as a function of Mach number. Each stage has a maximum pressure ratio of about 2. At $M = 4.60$, the overall compression ratio reaches a maximum value of 17.2.

In figure 20, the overall compression ratio $p_{t,TS}/p_{t,i,1}$ is plotted as a function of the total corrected mass flow entering the first-stage compressors. This form of presentation is used later to discuss the mass flow matching of the compressor system and the test-section diffuser system. It is again evident in this figure that during mode 2-IV operation, compressor G is operating in a choked mode (constant value of inlet mass flow) except at the maximum compression ratio point, which occurs at $M = 4.60$. This choked condition forces all the other compressors to operate at constant conditions from $M = 3.85$ to 4.45 and provides an opportunity to check the repeatability of the data presented in this report. These data are tabulated below and show that the repeatability is very good.

M_{TS}	$p_{t,TS}$, kPa	Compressor C			Compressor E			Compressor F		
		$\frac{w\sqrt{\theta_i}}{\delta_i}$, kg/sec	CR	$\frac{\Delta T_t}{T_{t,i}}$	$\frac{w\sqrt{\theta_i}}{\delta_i}$, kg/sec	CR	$\frac{\Delta T_t}{T_{t,i}}$	$\frac{w\sqrt{\theta_i}}{\delta_i}$, kg/sec	CR	$\frac{\Delta T_t}{T_{t,i}}$
3.85	131.1	144	2.00	0.336	151	1.99	0.325	77.1	2.11	0.324
4.00	141.3	144	1.99	.344	151	1.99	.324	77.6	2.11	.324
4.15	152.1	145	1.99	.344	153	1.99	.326	78.0	2.11	.326
4.30	163.0	144	1.99	.337	151	1.98	.326	77.6	2.10	.326
4.45	175.0	144	2.00	.340	152	1.99	.324	77.6	2.10	.324
4.60	187.1	139	1.99	.343	147	2.01	.320	73.9	2.10	.320

After the air has been discharged from each compressor, it enters a diffuser which decelerates the airflow velocity prior to its entry into a cooler, followed by the ducting which leads either to the next stage of compression or to a test section. The schematic drawings in figure 7 illustrate these components and flow paths. The total pressure losses which occur as the air passes through these components are shown in figure 21. In this figure, the inlet and exit total pressures for each stage of compression, referenced to the test-section total pressure, are plotted as a function of the test-section Mach number. Data for mode 1-II operation are not presented in the figure to simplify the data presentation. A small but consistent loss of total pressure occurs between the exit of each compressor and the inlet to the succeeding stage. Likewise, a pressure loss occurs between the exit from the last stage and the test section. At $M = 3.85$ this loss is largest, equal to about 3.7 percent of the test-section total pressure. Although the trend is not always apparent in figure 21, these losses are largest at the lowest Mach number of each operational mode and decrease as the Mach number in each mode increases.

For a given duct system, the above losses are a function of the flow dynamic pressure through the components and should, therefore, be a function of the Mach number at the compressor exit measuring station. In equation form, the total pressure loss, Δp_t, can be expressed as

$$\Delta p_t \propto q_d$$

$$\frac{\Delta p_t}{p_{t,d}} \propto \frac{\gamma}{2}(pM^2)_d \frac{1}{p_{t,d}} = K\left(\frac{p}{p_t}\right)_d M_d^2$$

where K includes the loss coefficient of each duct system. This equation is, of course, a very elementary, first-order representation of the actual pressure-loss phenomena.

All the ducting loss data are presented in figure 22. The total pressure loss through each section of ducting divided by the total pressure of the air entering the duct is plotted as a function of the corrected mass flow per unit area at the duct measuring station. This flow parameter is a unique function of the compressor discharge Mach number, as is shown in figure 22(a). The losses which occur between the discharge from the last stage of compression and the test section are plotted in

figure 22(b). Dashed curves indicate the loss values for K = 0.5 and 1.0. All the data correlate surprisingly well except those for the mode 1-II operation. The extra losses during this mode of operation may originate from the dump-turn of the ducting which occurs downstream of valve VIII (fig. 7(b)). Note that the average K value for each operating mode is tabulated with the symbol definition.

The interstage ducting losses are shown in figure 22(c). Each set of ducting has its own, reasonably consistent, value of K. The compressor-C-to-E interstage ducting exhibits a lower average value of K during mode 2-IV operation than during the other modes. This reduction of losses may occur because there is no airflow from compressor I being discharged into the ducting downstream of cooler 1 at 90° to the airflow from compressors C and D.

Electrical energy requirements.- The measured power input to the main drive motor system is indicated by the plotted data in figure 23. It should be noted that the electrical meter hookup is such that approximately 2 MW of indicated energy is consumed by some of the tunnel auxiliary systems. The power level varies from about 14 to 22 MW. At each mode change, a discontinuous increase in the power consumption occurs as another stage of compression is required to drive the test-section airflow. The calculated energy from figure 14, which each stage of compression inputs to the test-section airstream, is also shown in figure 23 by the shaded areas. Note that at a given Mach number, each stage of compression adds an approximately equal amount of energy to the test-section airstream. This would be expected since the temperature rise through all the compressors is about equal and independent of Mach number. The energy consumption of each stage decreases with increasing Mach number because the absolute mass flow of air through the test section is decreasing (fig. 12).

As would be expected, the measured energy input into the drive system is always larger than the energy input into the test-section airflow. However, at the lower Mach numbers, the differences are very large. For example, during mode 1-IA operation, the energy input to the drive system is from 75 to 100 percent larger than the input to the test-section airflow. As additional stages are added to provide the required compression ratio, the differences between the measured and calculated power levels gradually decrease. During mode 2-IV operation, the difference between the two energy quantities decreases to 15 percent. It is obvious that most of this energy difference must be absorbed by the bypassing compressors. Unfortunately, no instrumentation was available for the measurement of the bypass mass flows. Consequently, the energy absorption by these compressors could not be directly calculated.

It was decided to attempt to determine the bypass power requirements by an indirect experimental method. With the tunnel operating at a fixed set of test-section conditions, the variation in the total energy input to the drive system was measured as the discharge pressure from one bypassing compressor or a combination of bypassing compressors was varied from atmospheric to a near vacuum pressure. By extrapolating these variations of total power input to zero discharge pressure, it was possible to establish increments of bypass energy requirements as a function of the discharge pressure from each bypassing compressor. The data obtained for individual compressors and combinations of compressors are plotted in figures 24 and 25, respectively. The data were obtained over a period of time as a part of normal research testing operations. In figure 24, the various symbols differentiate the sets of data obtained for the same compressor from separate runs. It is apparent that the scatter of the data for each compressor necessitated the use of several sets of data to obtain a reasonably accurate estimate of the bypass power requirements. With an atmospheric discharge pressure, the power requirements for compressors E, F, and G were 4.0, 2.75, and 1.0 MW, respectively. The power requirements appear to

vary linearly with the discharge pressure. All the compressors operate with a pressure ratio of about 2 (fig. 14), indicating that large pressure losses occur somewhere in each bypass circuit.

In figure 25, the data points indicate the measured power requirements when the discharge pressures were varied simultaneously in several combinations of bypassing compressors. The lines represent the power requirements which would be predicted by summing the requirements for each compressor from figure 24. The relatively good agreement between the measured and predicted performances provides further assurance of the accuracy of the data shown in figure 24.

Using the information presented in figure 24, it is now possible to determine approximate values of the energy which would have to be input to the main drive system if all bypass power requirements could be eliminated from the data presented in figure 23. The results are shown in figure 26. For operating modes 1-IA, 1-II, and 2-II, most of the difference between the measured energy input to the main drive system and the calculated input to the test-section airflow is due, as expected, to the energy absorbed by the bypassing compressors. It would be expected that the increment between the calculated energy inputs to the airflow, and the measured energy inputs minus the bypass energy values (solid symbols) would be about constant across the Mach number range, since this increment represents primarily the inefficiency of converting electrical energy into mechanical energy and the power going to tunnel auxiliary systems. The reasons for the occurrence of a smaller increment during mode 1-IA operation are not understood.

It should be noted that an auxiliary vacuum system to facilitate pressure control in the bypassing compressor loops was included in the fiscal year 1979 facility rehabilitation program and should be operational by late 1981. Inclusion of this system will allow continuous operation of the bypassing compressors at a discharge pressure of about 34 kPa (1/3 atm) or less (if main drive vibrations are not encountered), and electrical requirements of the facility could be reduced as much as 10 percent.

Diffuser System Performance

General.- An analysis of the diffuser system performance is desirable because of its possible impact on the maximum Mach number capabilities and energy requirements of the facility. Two primary performance considerations are the maximum performance potential of the system and the actual performance as dictated by the mass-flow-matching characteristics of the compressor and the test-section diffuser system. Both these subjects are discussed in detail in references 2 to 5.

Wind-tunnel diffuser performance is generally measured as the ratio of the total pressure at the end of the diffuser to the test-section total pressure. During the present study, pressures were not measured at the end of the diffuser. It is, therefore, necessary to assume in the following discussion that the total pressure at the inlet to the first stage of compression is equal to the diffuser exit total pressure. With this assumption, the diffuser pressure recovery is equal to $p_{t,i,1}/p_{t,TS}$, the reciprocal of the overall compression ratio.

Schematic drawings of the variable-geometry systems which follow both test sections are shown in figure 8. The two systems are very similar. Since test section 2 covers a major portion of the total Mach number range of the tunnel, only the performance of this diffuser system will be discussed.

Maximum performance potential.- The primary parameter which determines the maximum performance of a variable-geometry diffuser system, assuming there are no other limiting conditions, is the contraction of the second-minimum flow area relative to the test-section area, A_{TS}/A_{SM}. As this parameter becomes larger, the minimum Mach number at which the diffuser normal shock system may occur becomes smaller, and the maximum attainable recovery becomes larger. In figure 27, the normal operating half-widths of the second minimum are plotted as a function of Mach number. These values have been selected over the years on the basis of extensive operational experience.

The average contraction ratios of the second minimum, based on the faired curve from figure 27 and a test-section reference area of 1.579 m^2, are shown by the solid line in figure 28. The ratio varies from about 1.16 to 1.47 over the Mach number range from 2.30 to 4.60. As indicated by the discussion which follows, these contraction ratios are small for a system which has the capability for changing the contraction ratio after the test-section flow has been started. References 5 and 6 contain data describing the maximum contraction ratios which have been obtained in other small research tunnels. The long-dashed curve represents one such set of data from reference 6. These data were obtained from a model tunnel which contained a representative model support system with support sting and body of revolution positioned at 15° angle of attack. From a practical operational viewpoint, the UPWT diffuser would not be expected to operate at values near these maximum levels because of the danger of damaging a model or force balance if the diffuser and test section should unexpectedly unstart. The reference 6 curve is presented only to indicate that contraction ratios significantly larger than the UPWT values have been obtained. As a further basis of reference, the short-dashed curve indicates the theoretical maximum second-minimum contraction ratios at which a supersonic tunnel can be started. References 5 and 6 indicate that the maximum experimental starting values are equal to or larger than the theoretical values. It would be expected that the UPWT variable-geometry diffuser system would operate at values which lie between the limits defined by the two dashed curves, but as indicated by the solid line in figure 28, the actual running values are smaller than the lower limits defined by the short-dashed curve.

Reference 5 presents data which indicate that for the contraction ratios represented by the short-dashed curve in figure 28, the required compression ratios are about equal to the inverse of the theoretical pressure recovery across a normal shock at the test-section Mach number. Since the UPWT contraction ratios are smaller than the short-dashed curve values, the UPWT minimum compression ratio at a given Mach number should be somewhat larger than the theoretical normal shock values. As a matter of general interest, the minimum compression ratios for the long-dashed curve shown in figure 28 vary from about 0.7 of the theoretical normal shock value at $M = 2.5$ to about 0.38 at $M = 4.0$ and 4.5.

The above discussion has established the general level of the maximum pressure recovery (minimum compression ratio) at which the UPWT diffuser system can operate. Special tests would be required to obtain the data to document the actual maximum pressure recoveries which are attainable because no such data presently exist.

Actual performance.- During the wind-tunnel operation, the corrected mass flow at the exit of the diffuser must match the corrected mass flow at which the compressor system will operate. The requirements of the compressor system have already been presented in figure 20. The corrected mass flow characteristics of the diffuser exit can be expressed by the following equations. The units of the constant 241.18 are kg/m^2-sec.

$$\left(\frac{w\sqrt{\theta}}{\delta}\right)_{i,1} = w_{TS}\left(\frac{\sqrt{\theta}}{\delta}\right)_{i,1} = 241.18\left(\frac{A_f}{A/A^*}\right)_{TS} \frac{p_{t,TS}}{p_{t,i,1}} \sqrt{\frac{T_{t,i,1}}{T_{t,TS}}} \qquad (1)$$

At a given test-section Mach number and constant operating temperature, the value of the corrected mass flow leaving the diffuser is proportional to the compression ratio $p_{t,TS}/p_{t,i,1}$ at which the system is operating. These characteristics, at typical test Mach numbers, have been superimposed on the compressor system characteristics in figure 29. The intersections of the two sets of curves represent the match points at which the system must operate. Physically, this matching is achieved by the shock system downstream of the second minimum adjusting its position in the diffuser until the necessary total pressure losses are generated. In other words, as the compression ratio increases at each test-section Mach number, the shock system moves downstream in the diffuser to higher supersonic Mach numbers and higher shock losses. The short-dashed curve on the left side of the figure represents the compresson ratios which are the reciprocals of the theoretical pressure recoveries of the test-section normal shock. As previously discussed, the minimum compression ratios at which the UPWT diffuser system can operate are probably somewhat higher than the normal shock values. As indicated by the other short-dashed line, the diffuser is actualiy operating at compression ratio levels which are about 40 percent higher than the normal shock levels. For the current Mach number range and operating procedures of the tunnel, there is obviously no advantage to be gained by attempting to improve the performance of the diffuser system because the airflow-matching characteristics of the tunnel and its drive system dictate that any diffuser system would have to operate at the same low levels of performance.

Some further insight into the performance of the diffuser can be obtained from the data presented in figure 30. In this figure, data obtained during the study to determine the effects of varying the inlet guide-vane position on compressor F have been added (solid symbols) to the data presented in figure 29. Data are presented for Mach numbers from 2.97 to 3.95 for guide-vane positions of 100, 80, and 60 percent open. Heavy broken lines have been faired through the 80- and 60-percent-open data. Four data points at the 100-percent-open position (M_{TS} = 2.97, 3.21, 3.45, and 3.73) are also plotted. No heavy line has been faired through these points since they are in very good agreement with the data from the current study. All the solid symbol data were obtained during mode 2-III operation. During these guide-vane effect studies, the upper Mach number limit of mode 2-III was extended from the normal value of 3.72 to 3.95. The higher Mach number data show that the diffuser system is capable of operation at efficiencies somewhat higher than the levels required by normal tunnel operations. At a Mach number slightly higher than 3.95, the flow in the diffuser and test section unstarted during operations at the 60- and 80 percent-open guide-vane positions. Unfortunately, the second-minimum positions for these data are unknown, and no significance, as far as diffuser performance is concerned, can be attached to the unstart Mach number.

One last bit of information can be gleaned from the data shown in figure 30. The minimum value of the first-stage inlet corrected mass flow is 245 kg/sec. Compressor C processes 37 percent, or 90.7 kg/sec, of this flow. This value is 19 percent lower than the minimum value shown in figure 16 and verifies that the stable operating range (fig. 17) for the 100-percent-open guide-vane position is at least as large as specified by the manufacturer.

Potential Performance Improvements

An improvement in tunnel performance, in terms of energy requirements, will probably be achieved with the completion of the installation of a new vacuum pump and control equipment that will allow independent pressure control in the bypassing compressor circuits. This savings can only be realized, of course, if main drive vibration problems are not encountered. Additional, but small, bypass power reductions may be achieved by operating these compressors at minimum temperature-rise conditions. This can be accomplished by operating at the minimum attainable inlet temperatures, which will vary with cooling tower performance, and by operating at the inlet guide-vane position which produces the smallest temperature-rise ratio $\Delta T_t/T_{t,i}$. It is not obvious from the available data that the lowest temperature-rise ratio occurs at the 40-percent-open guide-vane position. For example, in figure 18 at the 60-percent-open position, the temperature-rise ratio for compressor F is about 0.285. In figure 14(d) during bypass operation (40-percent-open position), the temperature-rise ratio varies from 0.32 to 0.34. Based on this set of data, less power is required by operation at the 60-percent-open position. Finally, the bypass power can also be reduced by operating the compressors at corrected airflow levels which are near the minimum values for stable airflow. No data are available to indicate that the compressors are, or are not, being operated at this condition.

Complete documentation of the performance of each of the compressors, as well as the combined system processing the test-section airflow, as a function of the inlet guide-vane position may uncover further procedures by which additional energy reductions may be realized. Analysis of such information may indicate that by reducing the inlet guide-vane angle, the temperature-rise ratio of some or all of the compressors driving the test-section air can be reduced without significantly increasing the likelihood of an unexpected unstart of the test section during normal test operation. For example, during mode 2-III operation, compressor F provides the third stage of compression and operates (fig. 14(d)) at a temperature-rise ratio of about 0.32 over the Mach number range from 3.00 to 3.70. The data of figure 18 indicate that with a 60-percent-open guide-vane position, the temperature-rise ratio is 0.28 for Mach numbers of 3.45 and 3.73 (corrected mass flow values of about 89 and 74 kg/sec, respectively). The corresponding energy reduction is 15 percent. During normal test operations at a Reynolds number of 6.56×10^6 per meter, compressor F absorbs an average of 6 MW over the 3.45 to 3.73 Mach number range (fig. 14(d)). The 15-percent energy reduction is equivalent to an overall energy reduction of 900 kWh for each hour of compressor F operation. It would appear from the matching data in figure 30 that compressor F could be operated with the guide vanes at the 60-percent-open position without significantly increasing the likelihood of a test-section unstart during normal mode 2-III test operations. It is, of course, impossible at this time to estimate the energy reductions which may be achieved from this type of approach. If an overall 5-percent reduction could be achieved from all compressors processing the test-section airflow, an energy reduction of about 1 million kWh/yr would result. As mentioned above, there is an increased possibility of encountering a tunnel unstart by operating with partially closed guide vanes if the overall compression ratio at a given Mach number is significantly reduced. However, the possibility of such an unstart could be minimized by installation in the tunnel of sufficient static pressure instrumentation to continuously monitor the position of the normal shock system relative to the diffuser second minimum. At the present time, the shock position is qualitatively monitored on the basis of the noise emanating from the diffuser section of the tunnel.

CONCLUDING REMARKS

A broad program to reduce the energy consumption of the Unitary Plan Wind Tunnel was initiated in 1973. As a part of this program, a study was made to determine if potential methods for increasing the operating efficiencies of the tunnel could be formulated. The study was conducted by determining the performance characteristics of the drive systems components and then analyzing the overall performance of the wind-tunnel system.

With the current (1977-1981) operating procedures, the power input to the test-section airflow is from 50 to 85 percent of the power input to the drive system. A major portion of the excess power is absorbed by the drive system compressors which are operating in a bypass mode to match the test-section airflow requirements in the Mach number range from 1.46 to 3.00. By late 1981, mechanical and control system improvements should allow the bypassing compressors to be operated at lower pressures if no adverse effects on main drive vibrations occur. This improvement could reduce the average energy requirements of the tunnel by as much as 10 percent. Additional small reductions in energy may be attainable by optimizing the compressor inlet guide-vane positions for both normal and bypass operation.

The operating-pressure-ratio characteristics of the tunnel are high relative to what should be attainable with an efficient variable-geometry diffuser system. These high pressure ratios are forced on the system by the airflow-matching characteristics of the test section and compressor system. Consequently, there is very little justification for attempting to improve the performance of the existing diffusers.

Langley Research Center
National Aeronautics and Space Administration
Hampton, VA 23665
August 7, 1981

APPENDIX

DERIVATION OF MASS FLOW EQUATION

The basic mass flow equation is

$$w = \rho A V$$

Writing the density ρ and the velocity V as functions of static pressure and static temperature gives the equation

$$w = \frac{p}{RT} AM\sqrt{\gamma RT} \times 10^3$$

The static pressure and the static temperature can be expressed as ratios to stagnation conditions by dividing and multiplying by p_t and T_t as follows.

$$w = \left(\frac{p}{p_t}\right) p_t AM\sqrt{\frac{\gamma}{R}} \frac{1}{\sqrt{\left(\frac{T}{T_t}\right)T_t}} \times 10^3$$

Since

$$\frac{p}{p_t} = \frac{1}{\left[1 + \left(\frac{\gamma - 1}{2}\right)M^2\right]^{3.5}}$$

$$\frac{T}{T_t} = \frac{1}{1 + \left(\frac{\gamma - 1}{2}\right)M^2}$$

$\gamma = 1.4$ for air

by substitution,

$$w = \sqrt{\frac{\gamma}{R}} AM \frac{p_t}{\sqrt{T_t}} \frac{\left(1 + 0.2M^2\right)^{0.5}}{\left(1 + 0.2M^2\right)^{3.5}} \times 10^3$$

$$w = \sqrt{\frac{\gamma}{R}} \frac{p_t}{\sqrt{T_t}} A \frac{M}{\left(1 + 0.2M^2\right)^{3.0}} \times 10^3$$

From reference 7, equation (80),

$$\frac{A}{A^*} = \frac{125}{216} \frac{\left(1 + 0.2M^2\right)^3}{M}$$

Therefore,

$$\frac{M}{\left(1 + 0.2M^2\right)^3} = \frac{125}{216} \frac{1}{(A/A^*)}$$

By substitution,

$$w = \sqrt{\frac{\gamma}{R}} \frac{125}{216} \frac{p_t A}{\sqrt{T_t}} \frac{1}{(A/A^*)} \times 10^3$$

Since $R = 287.05$ J/kg-K for air, and as noted above, $\gamma = 1.4$

$$w = \frac{40.41 p_t A}{(A/A^*)\sqrt{T_t}}$$

where the constant 40.41 has units of kg-$K^{1/2}$/N-sec, and the mass flow w is expressed in kilograms per second.

REFERENCES

1. Jackson, Charlie M., Jr.; Corlett, William A.; and Monta, William J.: Description and Calibration of the Langley Unitary Plan Wind Tunnel. NASA TP-1905, 1981.

2. Pope, Alan; and Goin, Kennith L.: High-Speed Wind Tunnel Testing. Robert E. Krieger Pub. Co., 1978.

3. Donovan, A. F.; Lawrence, H. R.; Goddard, F. E.; and Gilruth, R. R., eds.: High Speed Problems of Aircraft and Experimental Methods. Princeton Univ. Press, 1961.

4. Fejer, Andrew A.; and Clark, James: Compressors for High-Speed Wind Tunnels. AGARDograph 14, Jan. 1956.

5. Lukasiewicz, J.: Diffusers for Supersonic Wind Tunnels. J. Aeronaut. Sci., vol. 20, no. 9, Sept. 1953, pp. 617-626.

6. Hasel, Lowell E.; and Sinclair, Archibald R.: A Preliminary Investigation of Methods for Improving the Pressure-Recovery Characteristics of Variable-Geometry Supersonic-Subsonic Diffuser Systems. NACA RM L57H02, 1957.

7. Ames Research Staff: Equations, Tables, and Charts for Compressible Flow. NACA Rep. 1135, 1953. (Supersedes NACA TN 1428.)

TABLE I.- COMPRESSOR INLET STAGNATION PRESSURE MEASUREMENTS

Operating mode	Test-section Mach number	Test-section stagnation pressure, kPa	Compressor inlet stagnation pressure, kPa				
			I	C	E	F	G
1-IA	1.50	39.98	23.22	23.32			
	1.65	41.70	22.46	22.70			
	1.80	43.81	22.26	22.46			
	1.95	46.68	23.03	23.22			
	2.16	51.38	24.95	25.23			
1-II	2.35	56.79	22.50	22.70	44.62		
	2.50	61.05	21.12	21.40	42.13		
	2.65	65.93	19.97	20.11	39.69		
	2.80	71.39	19.54	19.73	38.93		
	2.85	73.93	19.68	19.87	39.41		
2-II	2.30	54.97	23.70	23.94	47.35		
	2.35	56.40	23.22	23.51	46.25		
	2.50	60.95	21.83	22.07	43.57		
	2.65	65.98	20.64	20.83	41.13		
	2.80	71.63	19.73	19.97	39.55		
	2.96	77.81	19.63	19.83	39.69		
2-III	3.00	79.53	17.67	17.81	34.95	50.42	
	3.15	86.14	16.57	16.76	32.80	48.65	
	3.30	93.18	15.56	15.66	30.69	48.79	
	3.45	100.8	14.70	14.84	28.97	49.65	
	3.60	108.8	14.27	14.46	28.25	52.14	
	3.70	114.3	14.17	14.32	28.30	54.44	
2-IV	3.85	131.1		14.70	28.68	56.16	116.0
	4.00	141.3		13.74	26.77	52.29	108.4
	4.15	152.1		12.78	24.80	48.50	100.4
	4.30	163.0		11.97	23.27	45.34	93.80
	4.45	175.0		11.25	21.88	42.90	88.67
	4.60	187.1		10.87	21.02	41.70	86.23

TABLE II.- INLET STATIC PRESSURE MEASUREMENTS FOR COMPRESSORS ON BYPASS

Operating mode	Test-section Mach number	Test-section stagnation pressure, kPa	Compressor inlet static pressure, kPa			
			I	E	F	G
1-IA	1.50	39.98		57.50	53.00	48.31
	1.65	41.70		55.64	53.10	48.31
	1.80	43.81		55.83	54.49	48.55
	1.95	46.68		57.17	53.39	48.55
	2.16	51.38		57.36	53.29	48.31
1-II	2.35	56.79			59.52	46.83
	2.50	61.05			59.37	46.83
	2.65	65.93			58.89	46.88
	2.80	71.39			58.65	46.73
	2.85	73.93			58.65	46.83
2-II	2.30	54.97			55.78	47.59
	2.35	56.40			55.78	47.35
	2.50	60.95			55.64	47.31
	2.65	65.98			55.59	47.21
	2.80	71.63			55.49	47.16
	2.96	77.81			55.49	47.16
2-III	3.00	79.53				44.86
	3.15	86.14				42.61
	3.30	93.18				41.80
	3.45	100.8				40.70
	3.60	108.8				39.74
	3.70	114.3				38.88
2-IV	3.85	131.1	18.19			
	4.00	141.3	16.95			
	4.15	152.1	15.70			
	4.30	163.0	14.75			
	4.45	175.0	13.84			
	4.60	187.1	13.36			

TABLE III.- COMPRESSOR INLET STAGNATION TEMPERATURE MEASUREMENTS

Operating mode	Test-section Mach number	Test-section stagnation temperature, K	Compressor inlet stagnation temperature, K				
			I	C	E	F	G
1-IA	1.50	339	299	296	316	304	307
	1.65	339	299	296	16	304	307
	1.80	339	299	296	6	304	307
	1.95	339	299	296	6	304	307
	2.16	339	299	297		302	296
1-II	2.35	339	300	297	304	304	308
	2.50	339	300	297	304	304	306
	2.65	339	301	298	306	304	308
	2.80	339	300	298	306	305	308
	2.85	339	301	298	306	306	308
2-II	2.30	339	303	301	311	314	312
	2.35	339	302	299	311	314	312
	2.50	339	302	299	311	314	311
	2.65	339	301	298	311	313	311
	2.80	339	300	298	310	313	311
	2.96	339	299	297	309	313	309
2-III	3.00	339	303	301	311	314	313
	3.15	339	303	301	312	315	313
	3.30	339	304	302	312	315	313
	3.45	339	305	303	312	315	314
	3.60	339	304	302	313	315	314
	3.70	339	304	302	312	314	314
2-IV	3.85	353	318	303	315	316	316
	4.00	353	311	302	316	316	316
	4.15	353	311	302	315	315	316
	4.30	353	312	303	316	316	316
	4.45	353	312	302	316	316	316
	4.60	353	312	302	316	316	316

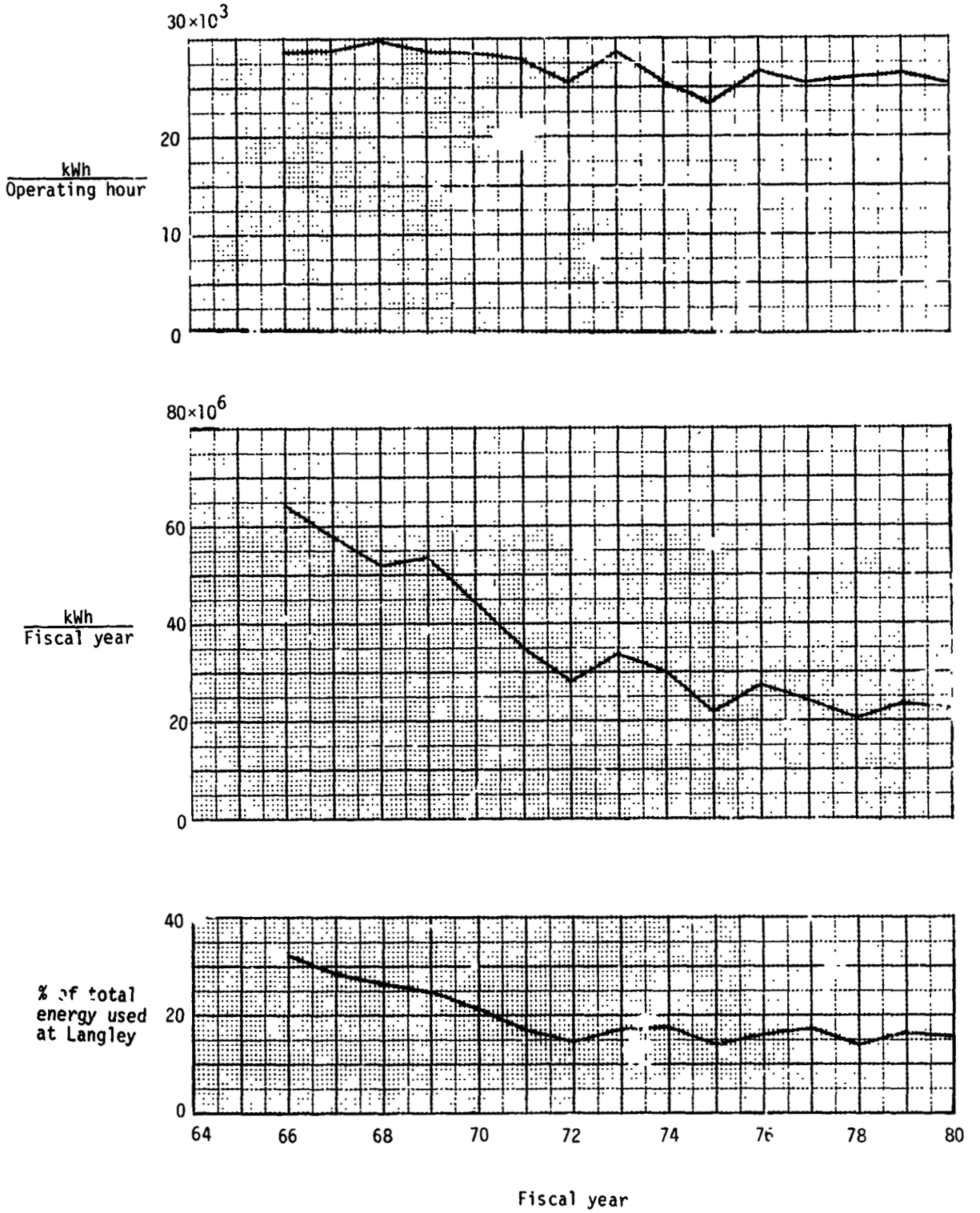

Figure 1.- Summary of electrical energy used by the Langley Unitary Plan Wind Tunnel.

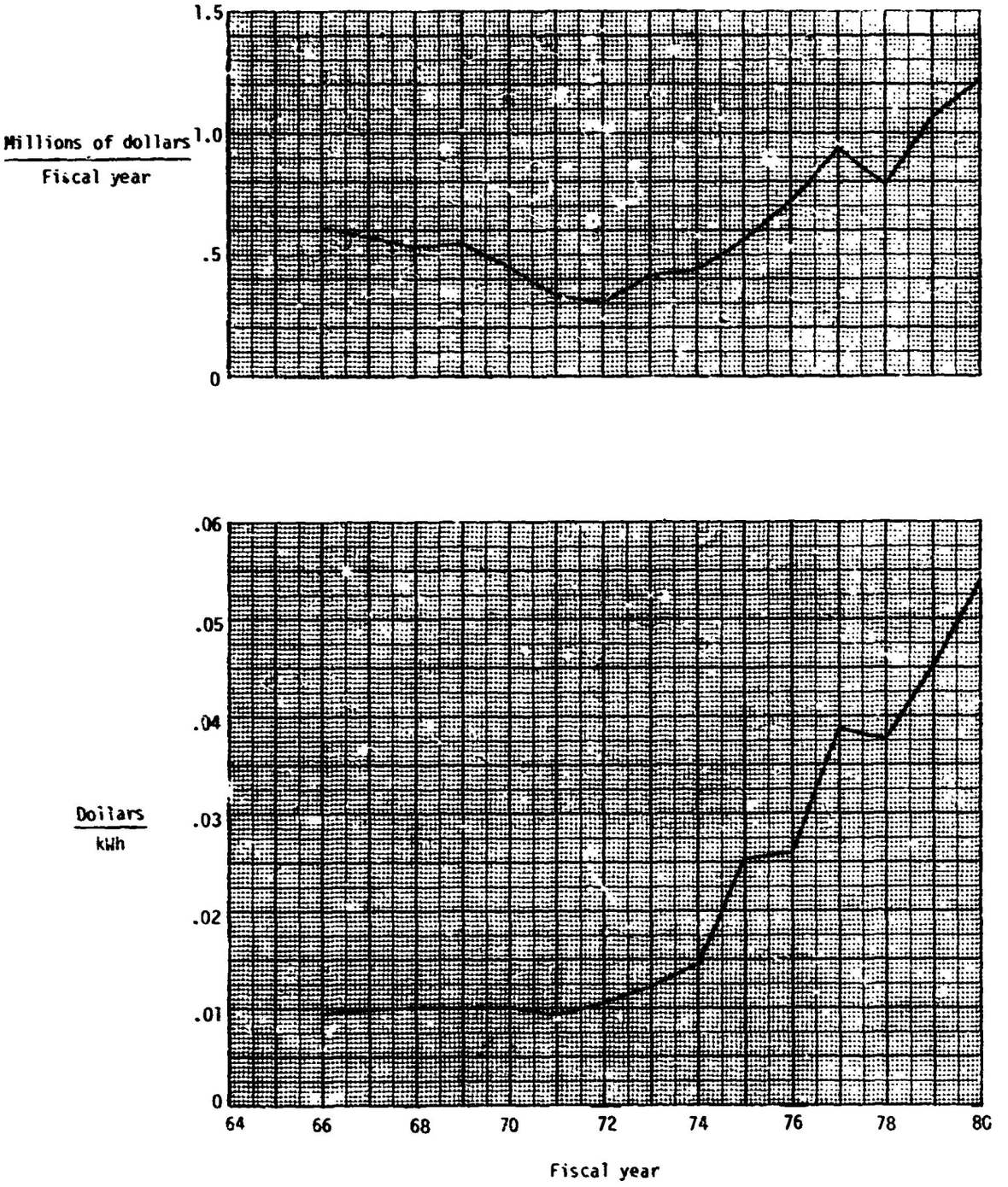

Figure 2.- Electrical energy costs for operation of the UPWT.

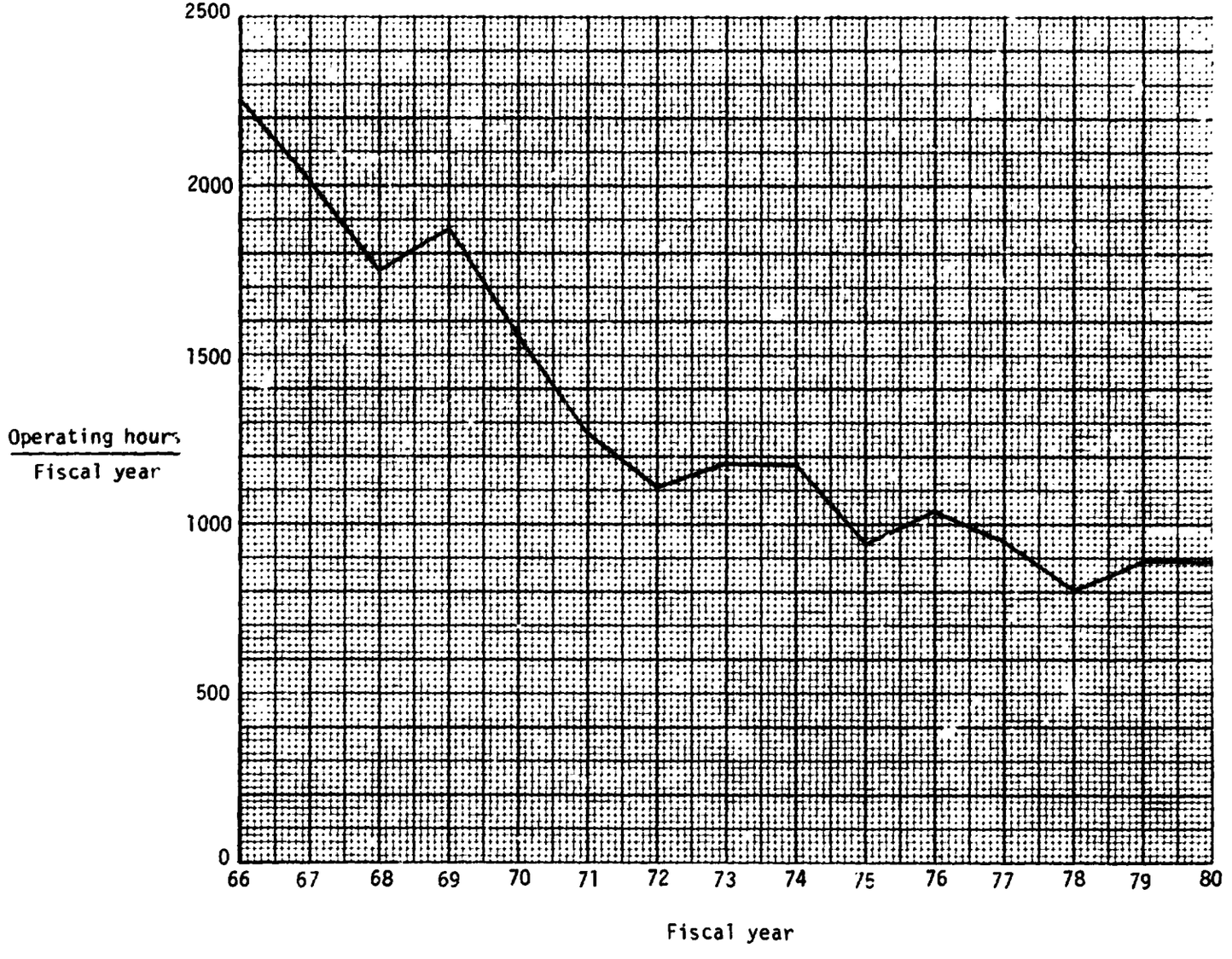

Figure 3.- Operating hours per year for the UPWT.

L-81-201

Figure 4.- Photograph of UPWT building.

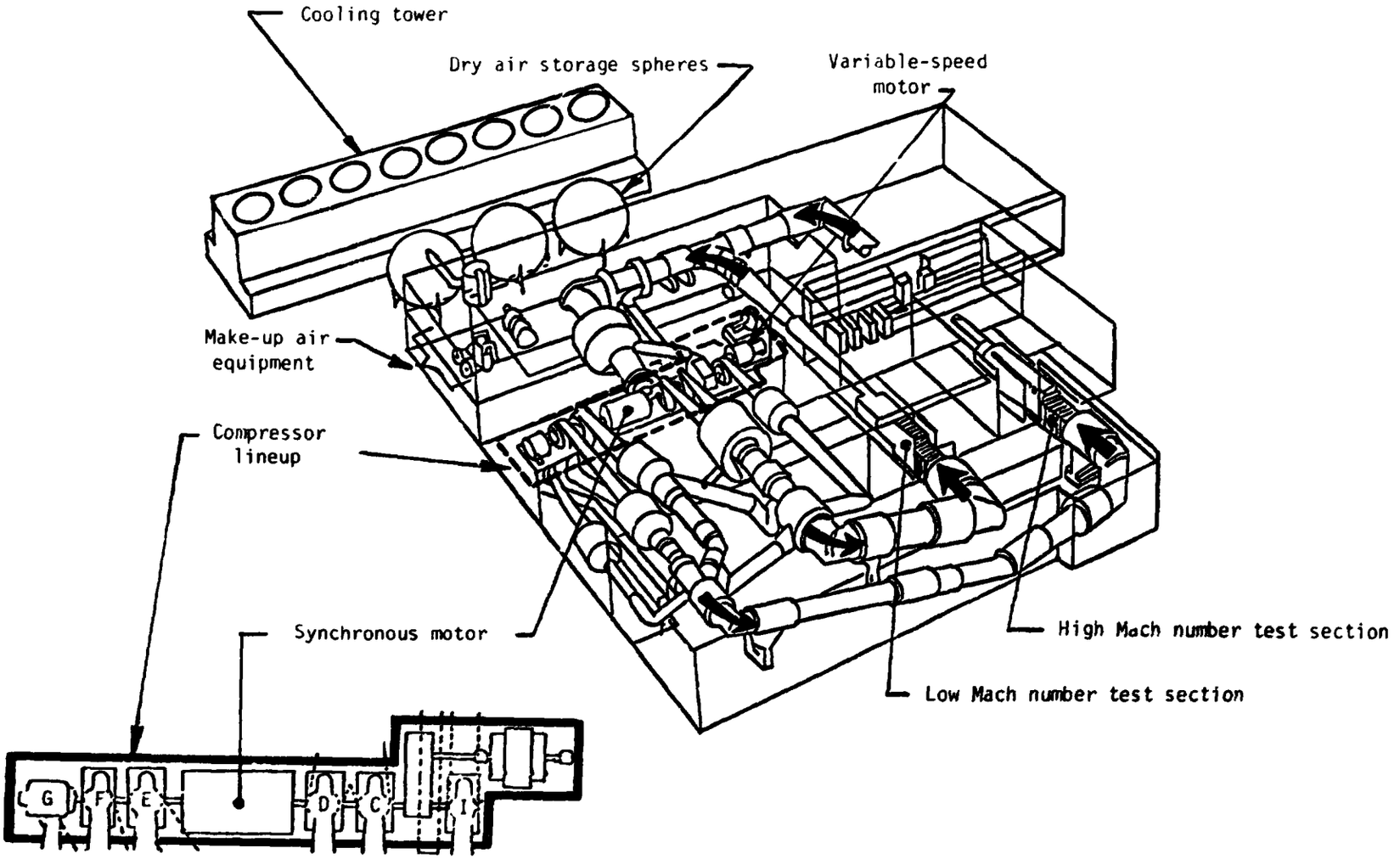

Figure 5.- Schematic drawing of Langley Unitary Plan Wind Tunnel.

L-81-202

Figure 6.- Photograph of UPWT main drive assembly.

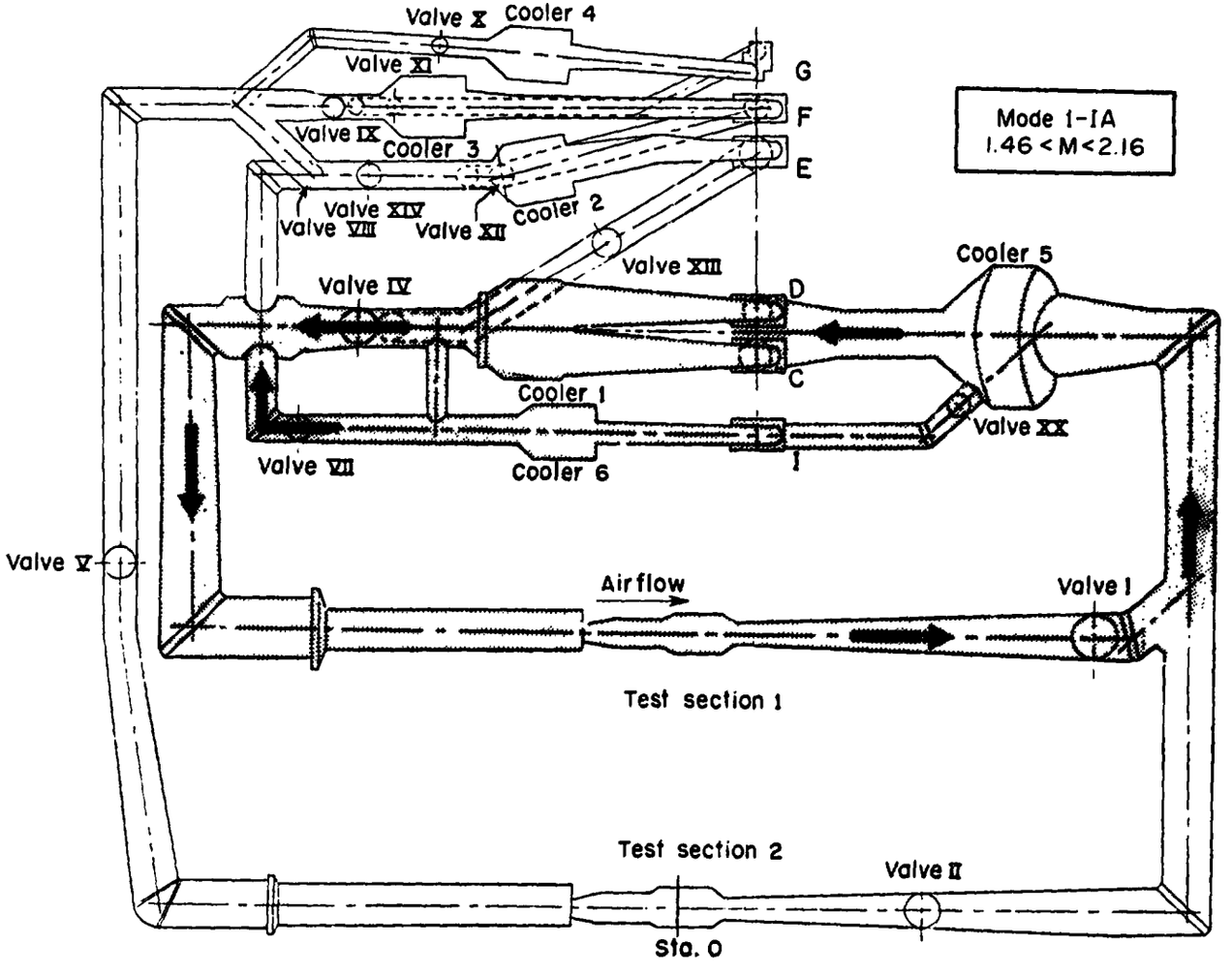

(a) Mode 1-IA.

Figure 7.- Tunnel operating circuit configurations.

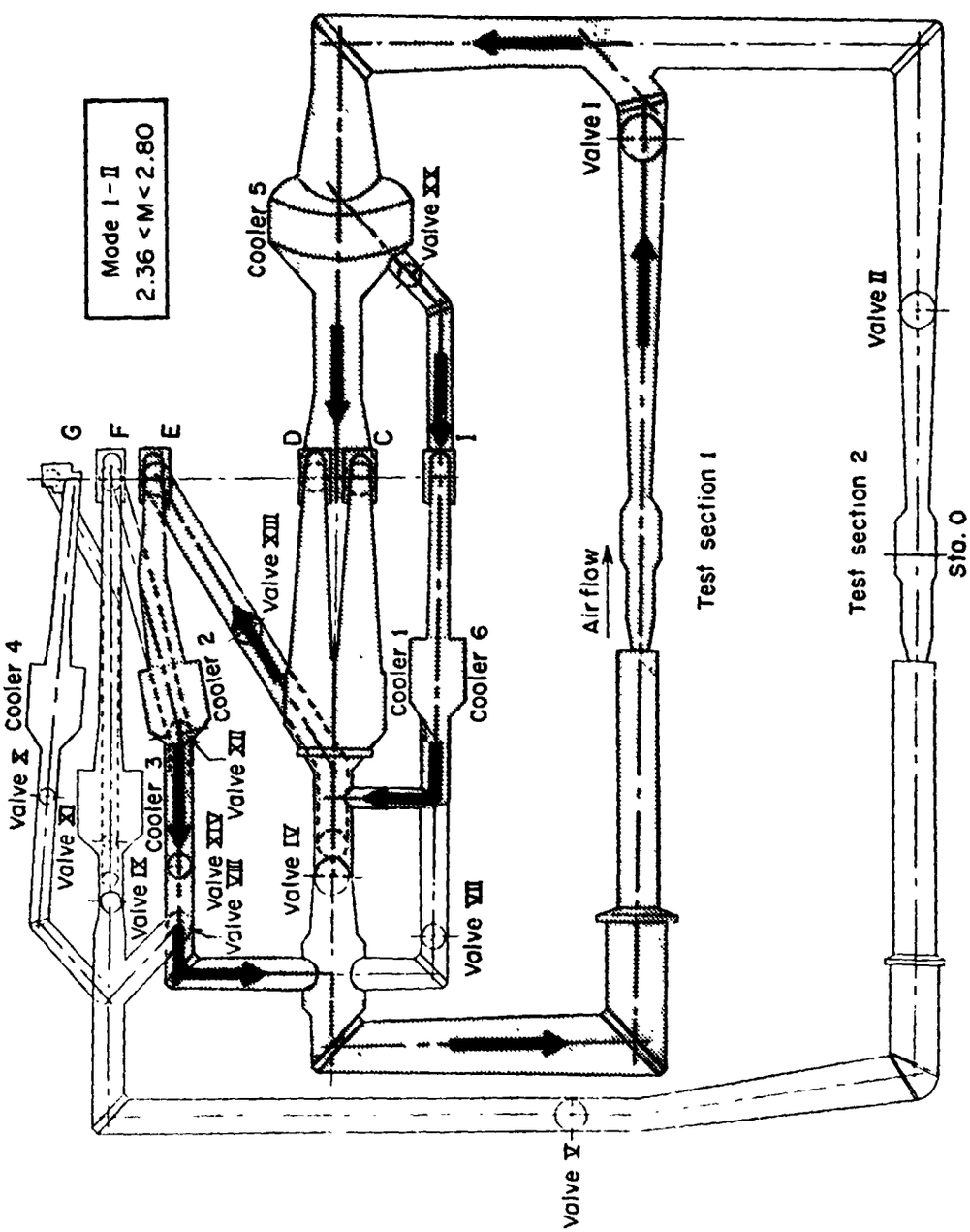

(b) Mode 1-II.

Figure 7.- Continued.

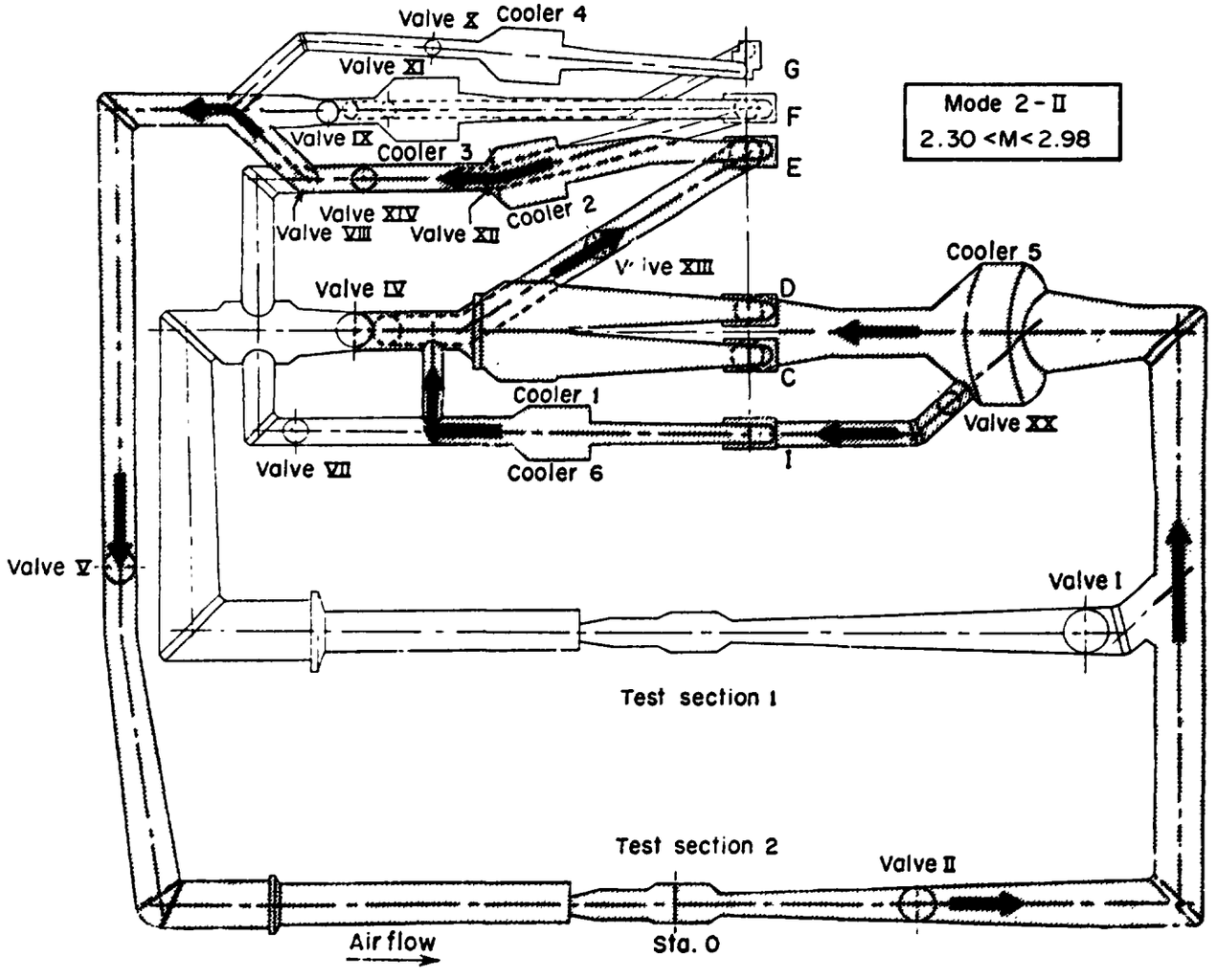

(c) Mode 2-II.

Figure 7.- Continued.

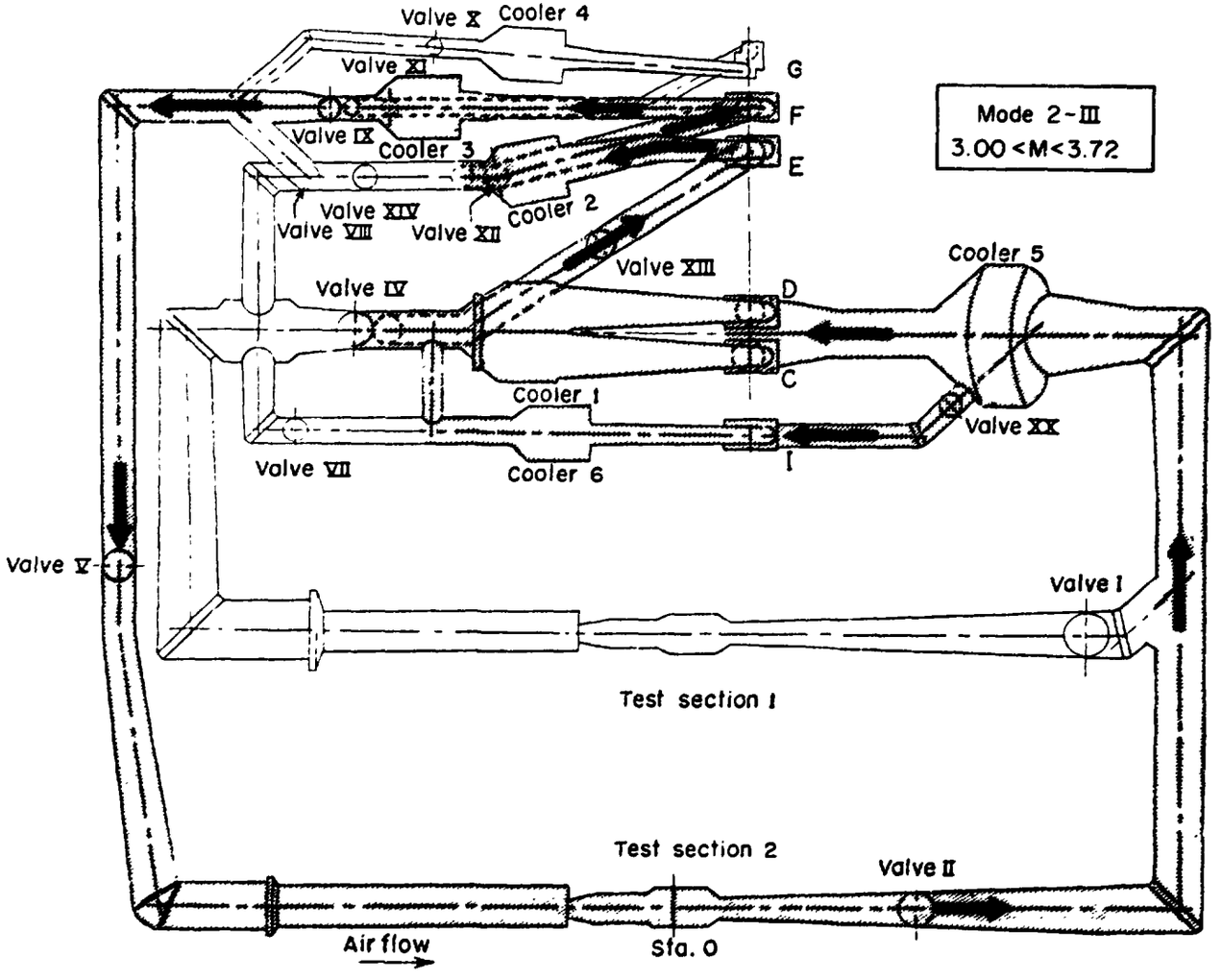

(d) Mode 2-III.

Figure 7.- Continued.

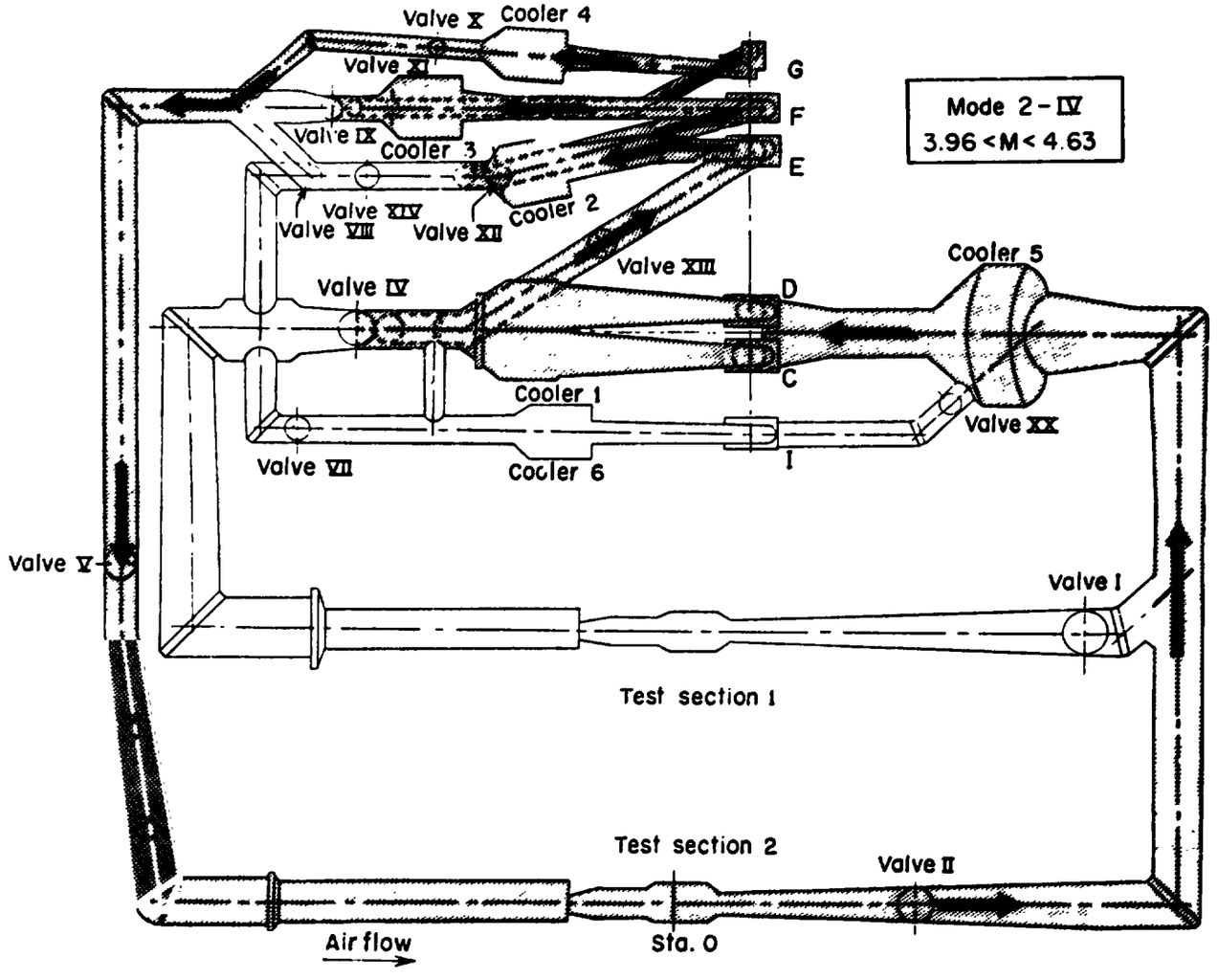

(e) Mode 2-IV.

Figure 7.- Concluded.

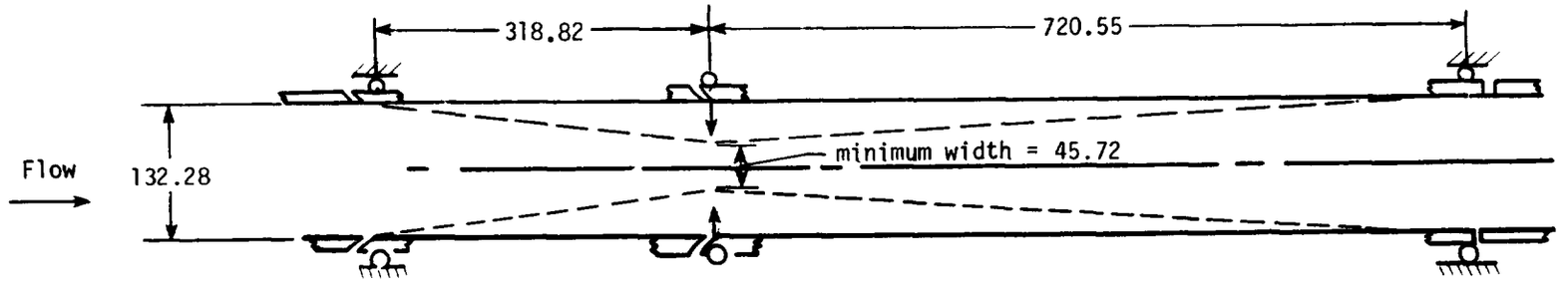

(a) Test section 1.

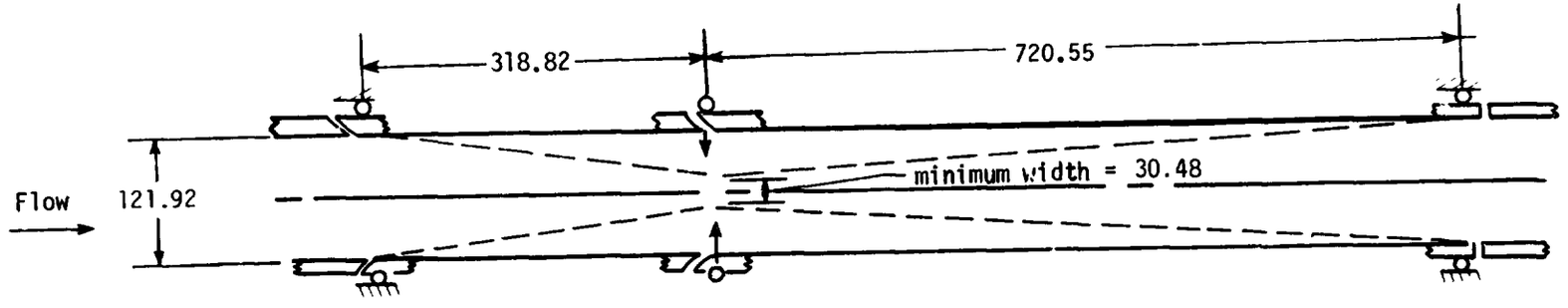

(b) Test section 2.

Figure 8.- Plan-view schematics of supersonic-subsonic, variable-geometry, diffuser systems. All dimensions in centimeters.

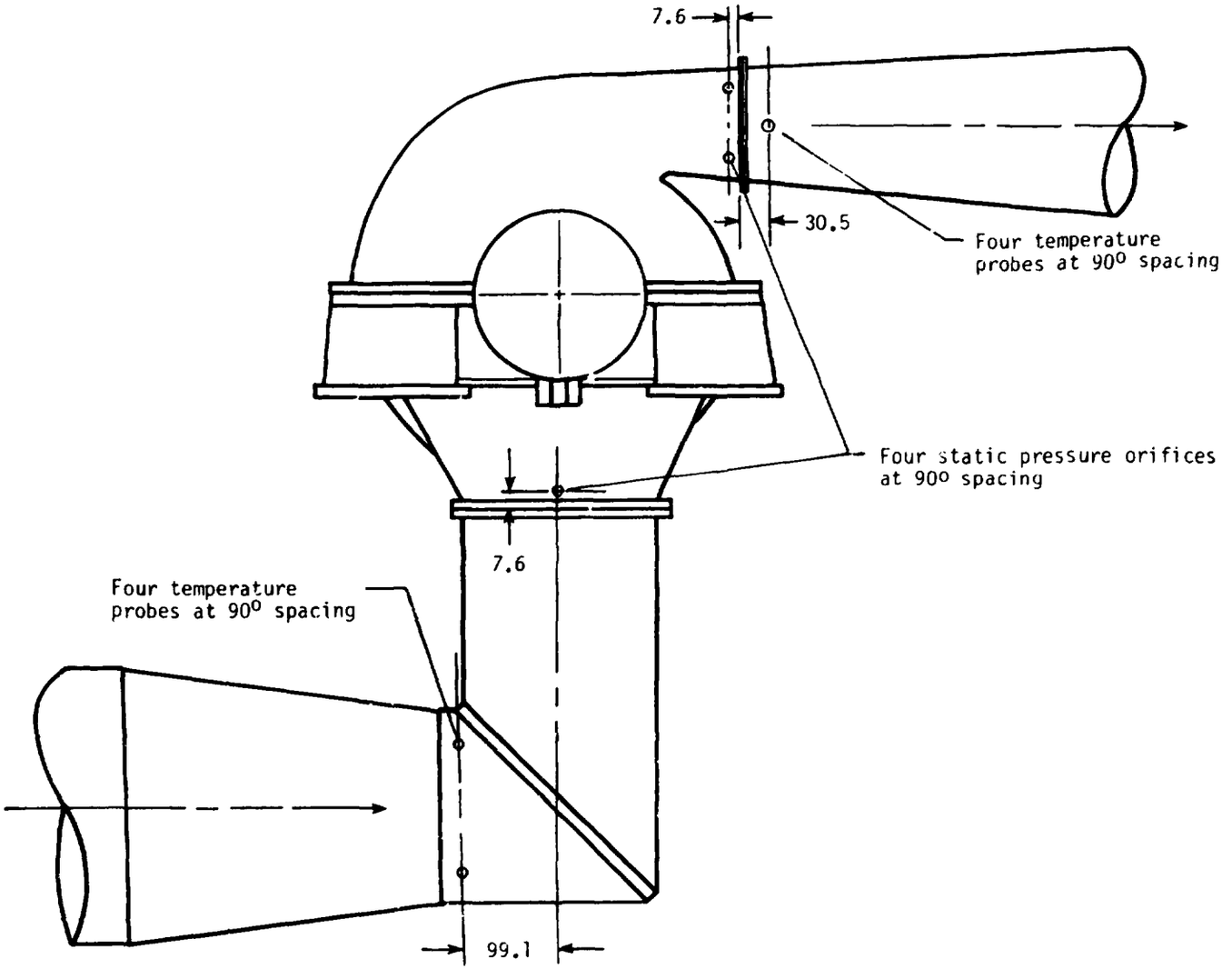

(a) Compressors C and D.

Figure 9.- Typical compressor instrumentation locations (all dimensions in centimeters).

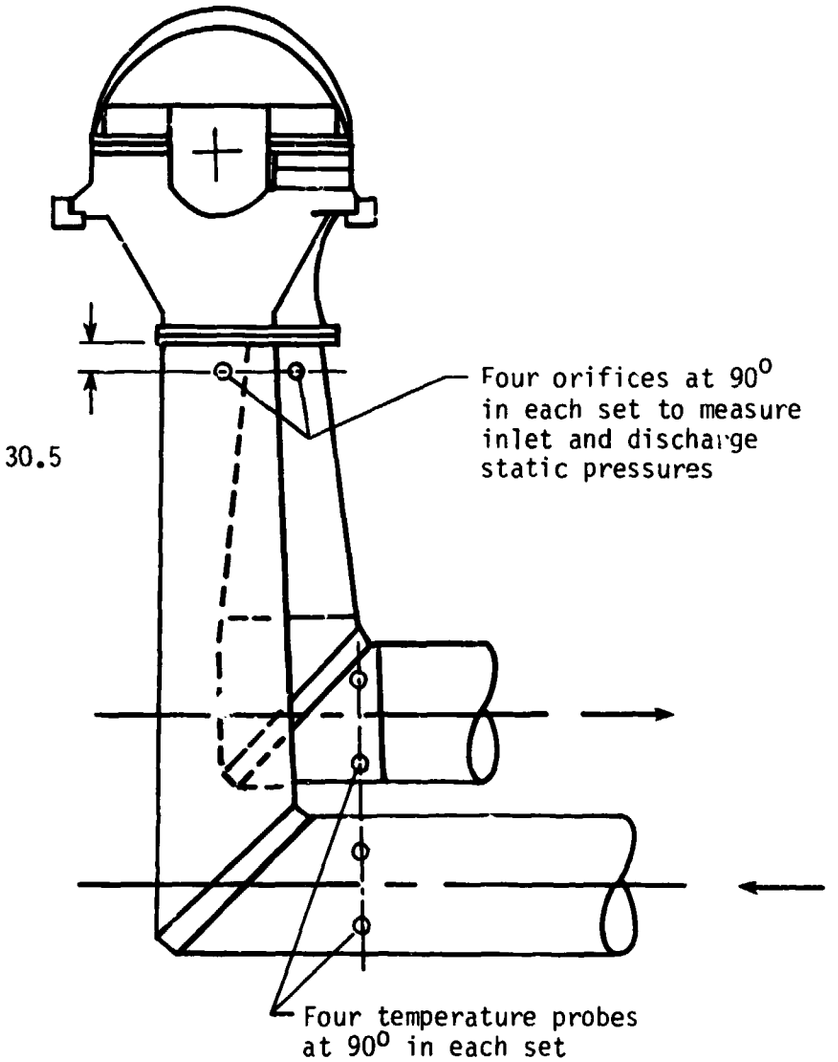

(b) Compressor G.

Figure 9.- Concluded.

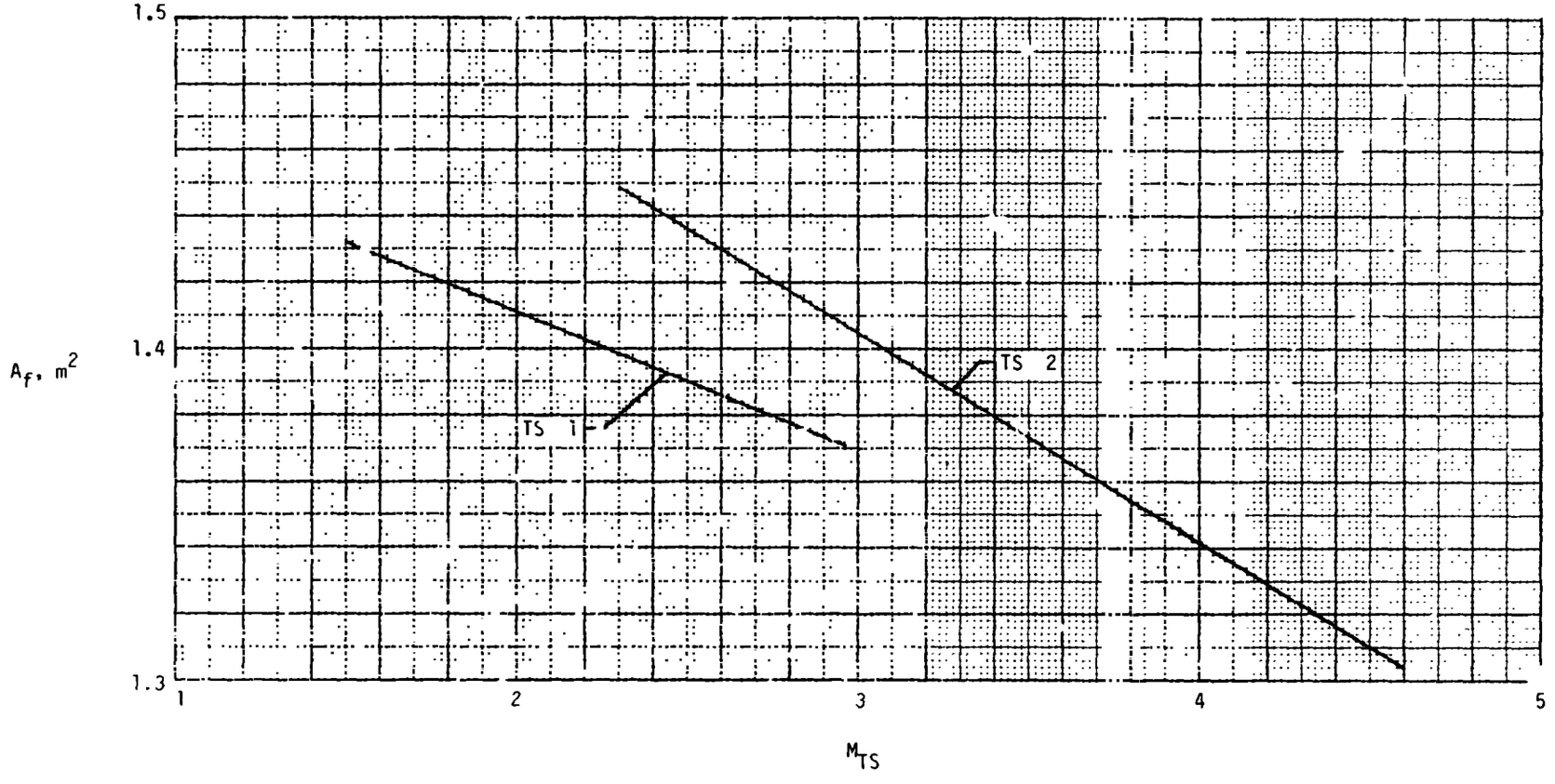

Figure 10.- Variation of test-section effective flow area with Mach number.

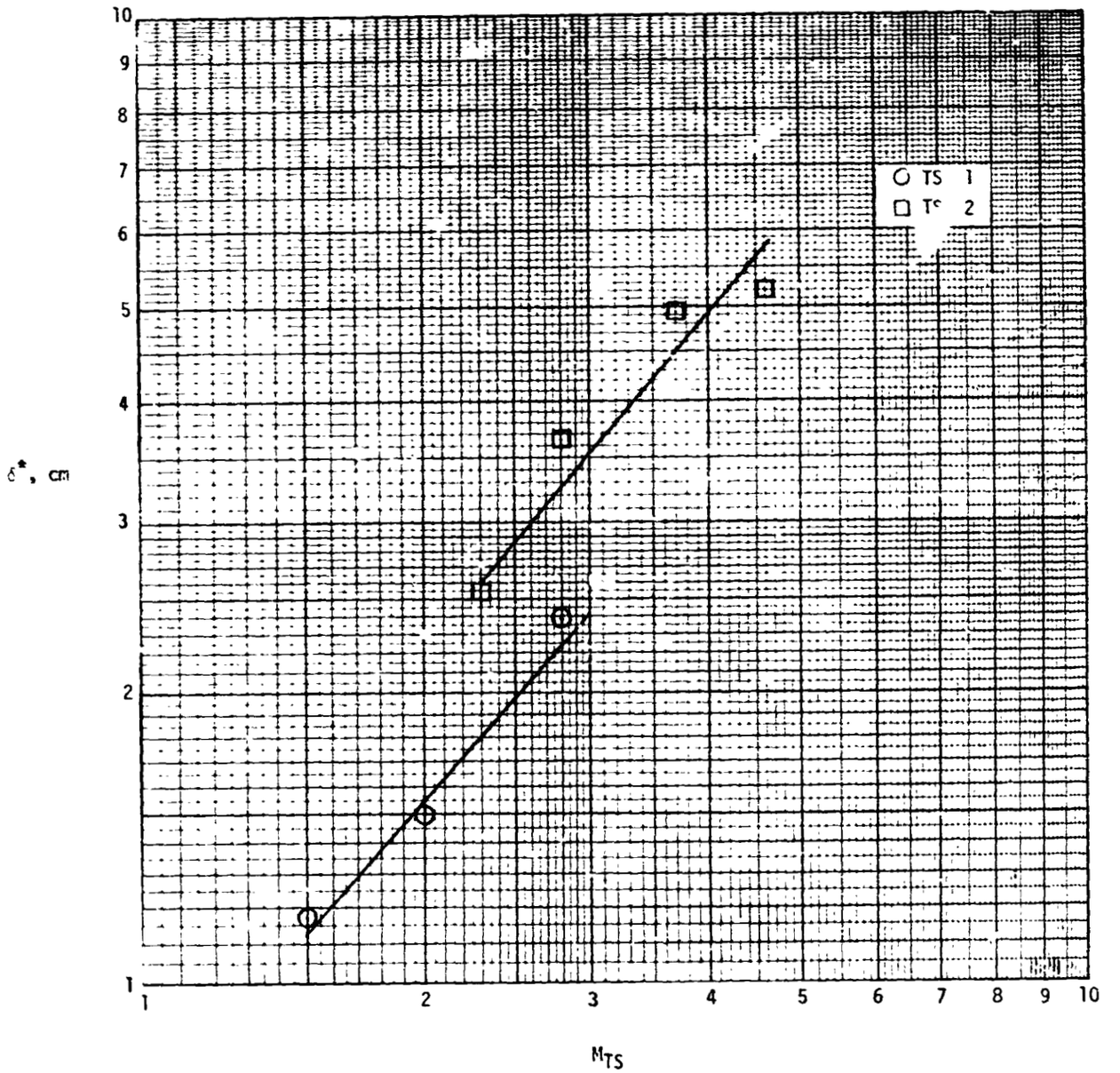

Figure 11.- Variation of test-section sidewall boundary-layer displacement thickness with Mach number.

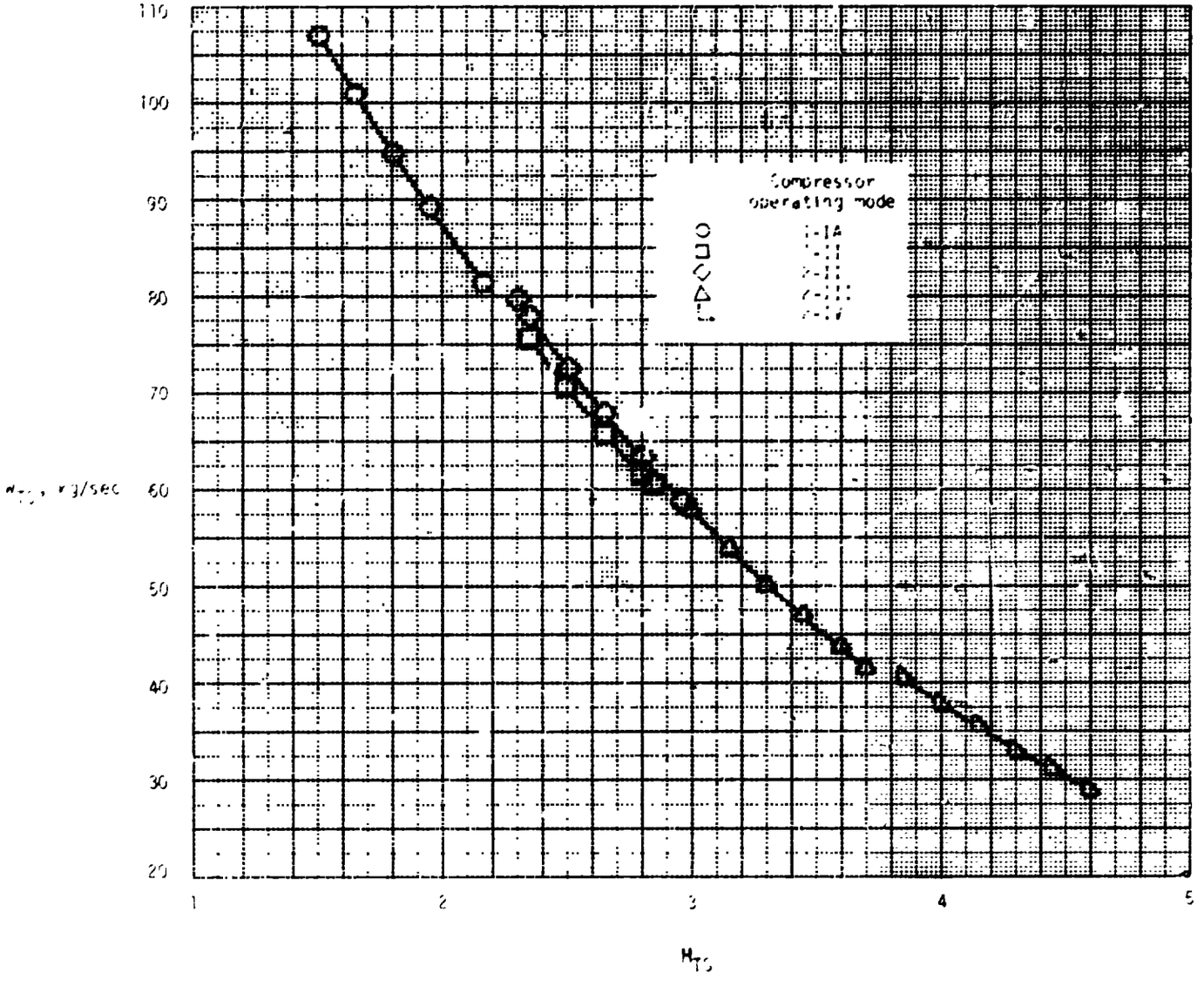

Figure 12.- Variation of calculated mass flow with Mach number.

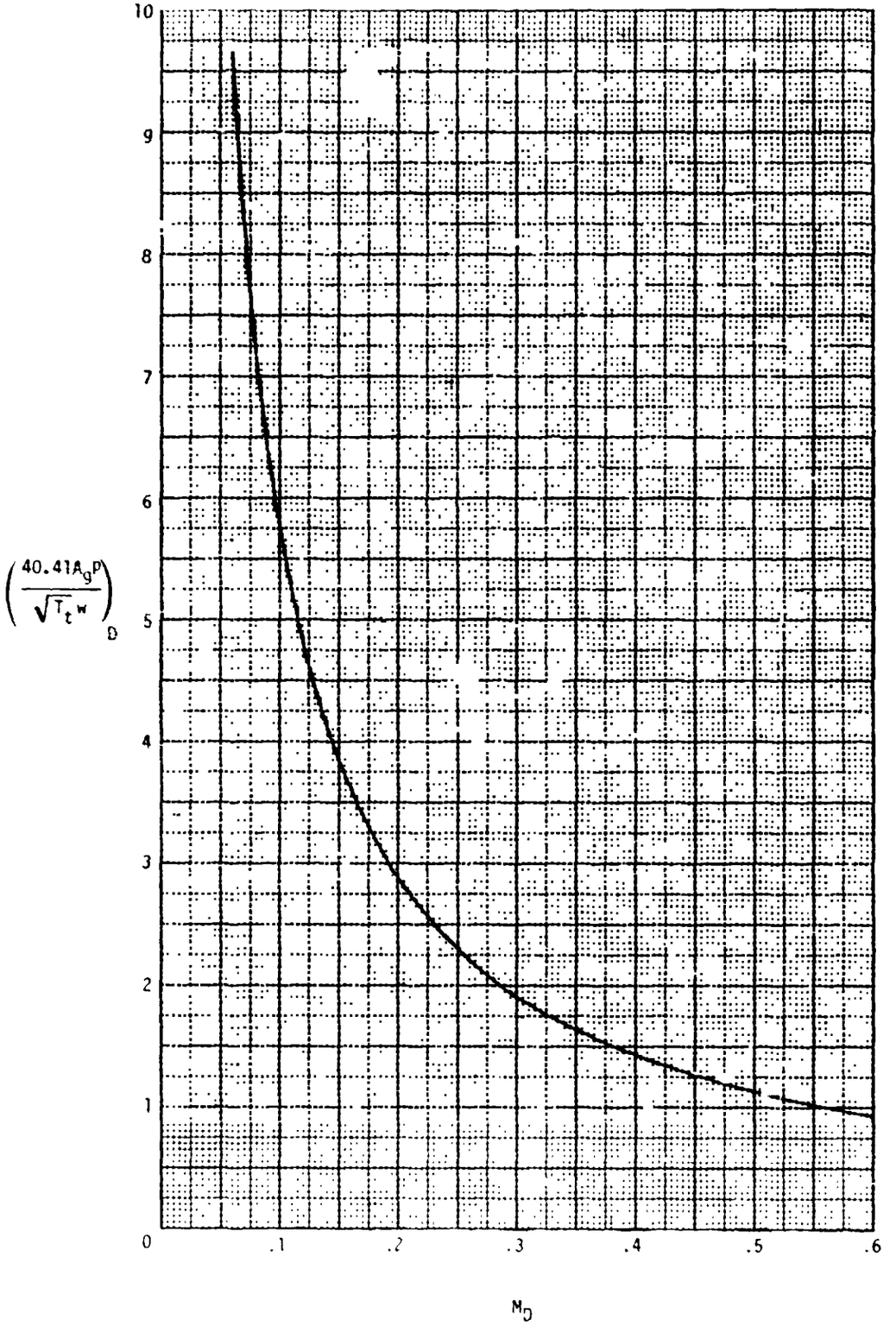

Figure 13.- Curve for evaluating duct Mach number from known duct parameters A_g, p, T_t, and w.

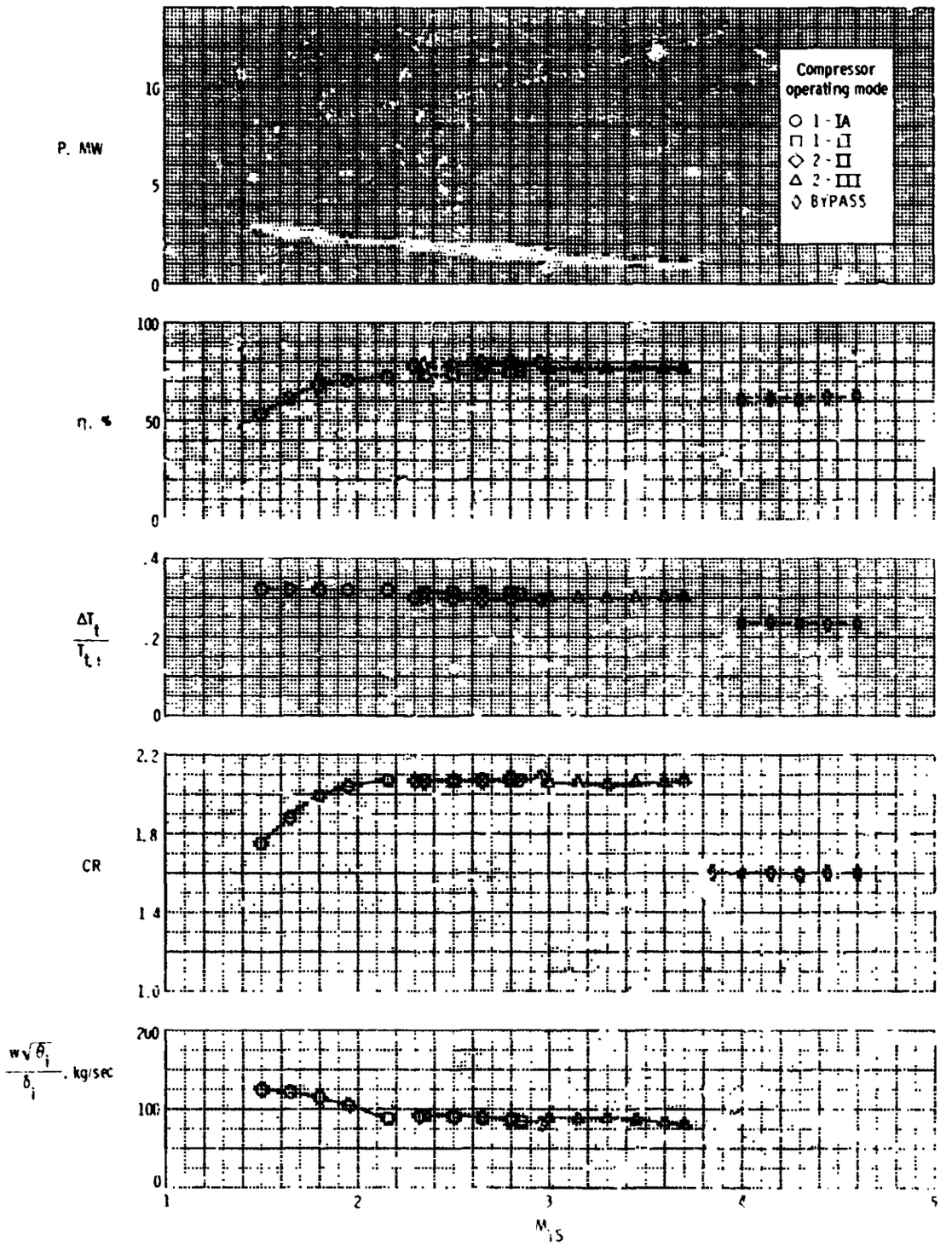

(a) Compressor I.

Figure 14.- Measured performance of compressors.

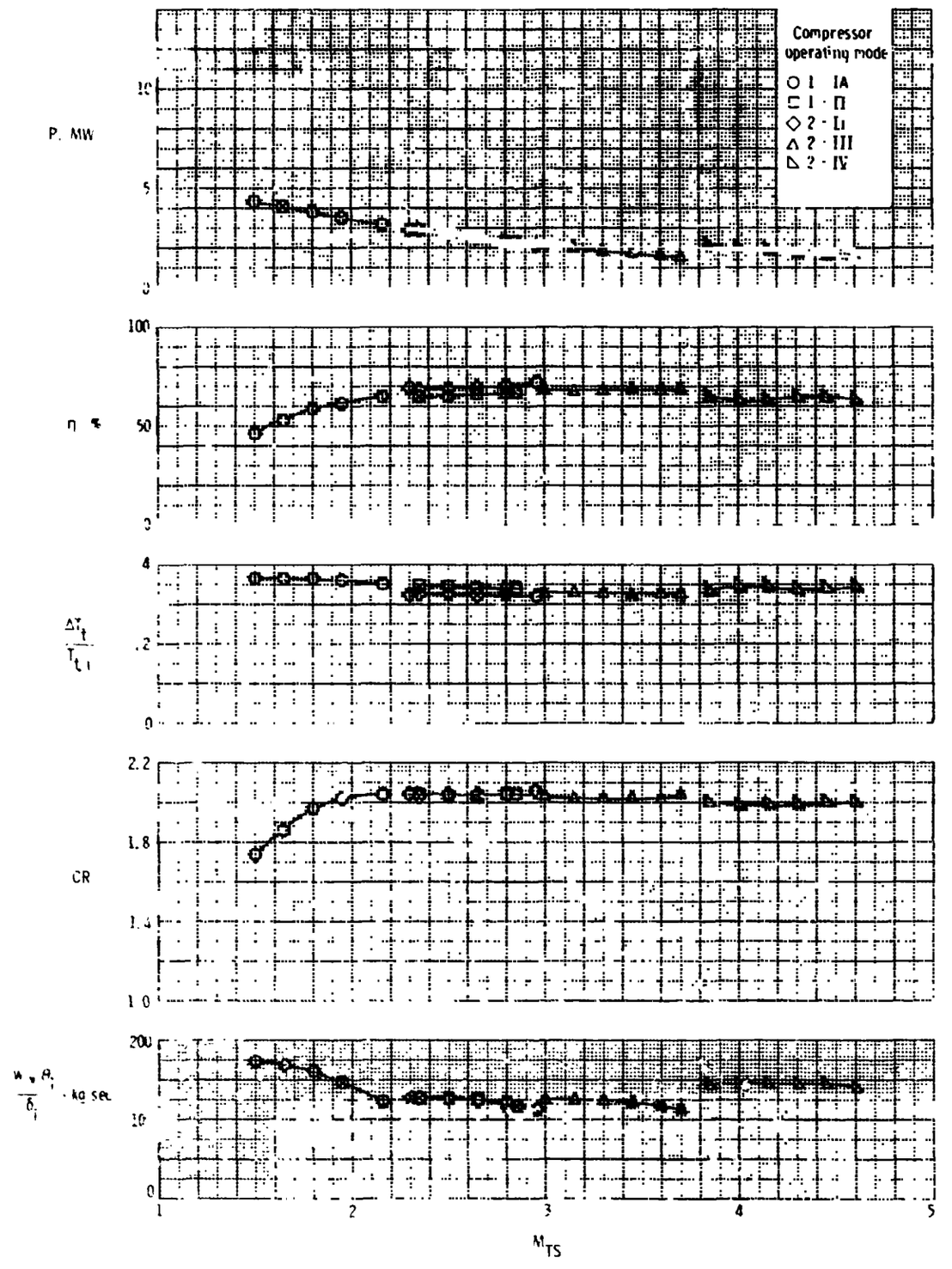

(b) Compressor C.

Figure 14.- Continued.

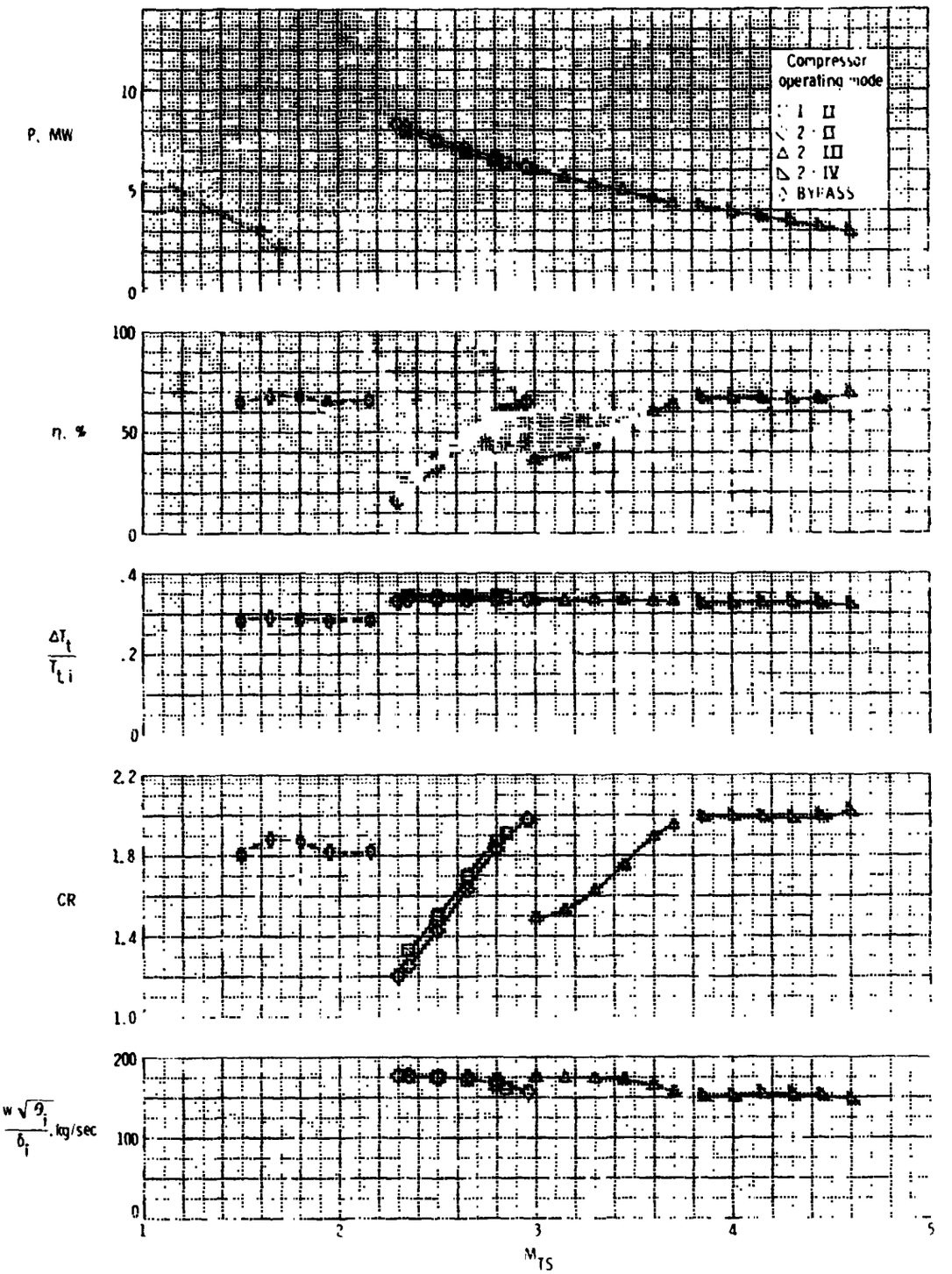

(c) Compressor E.

Figure 14.- Continued.

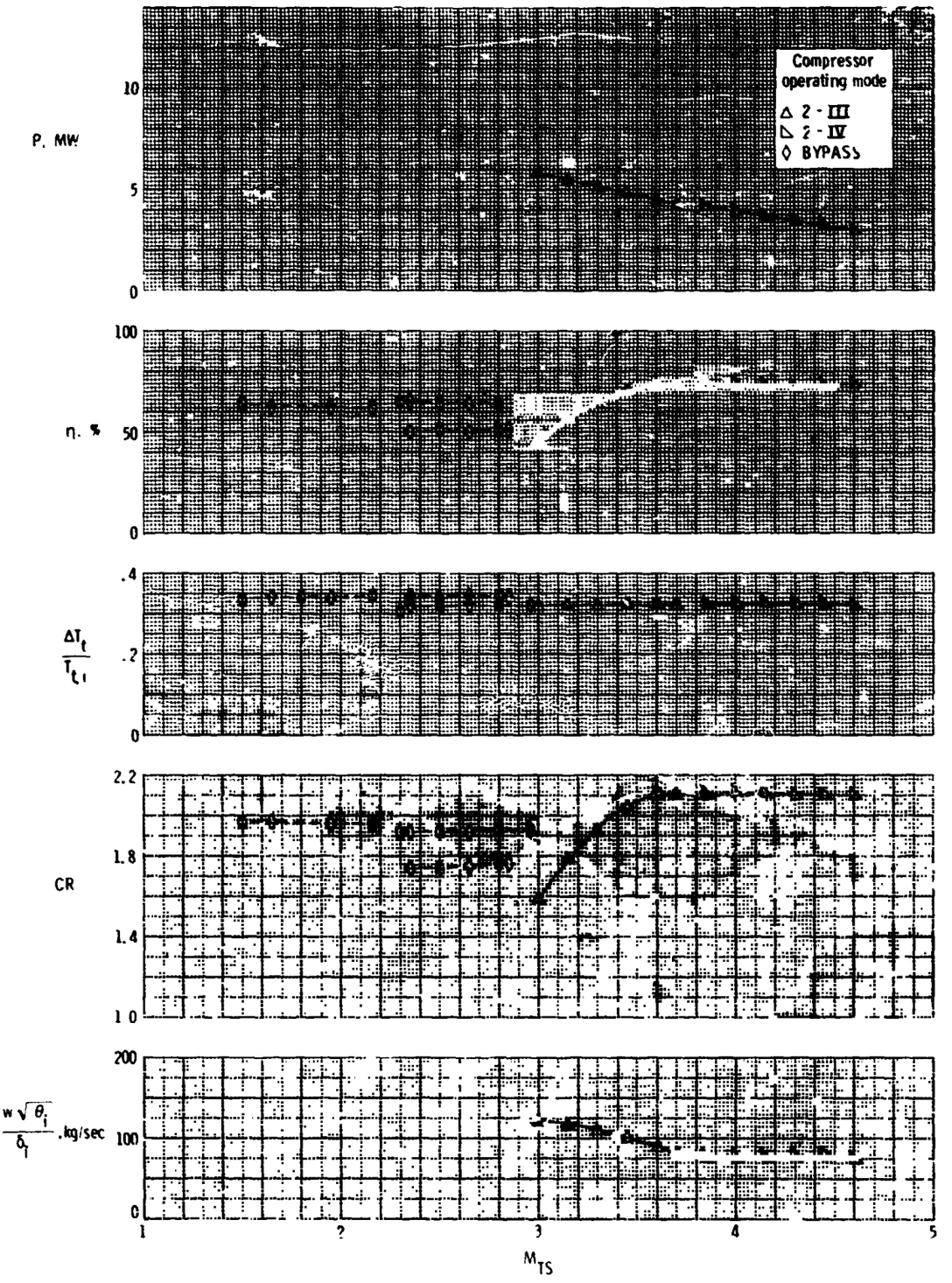

(d) Compressor F.

Figure 14.- Continued.

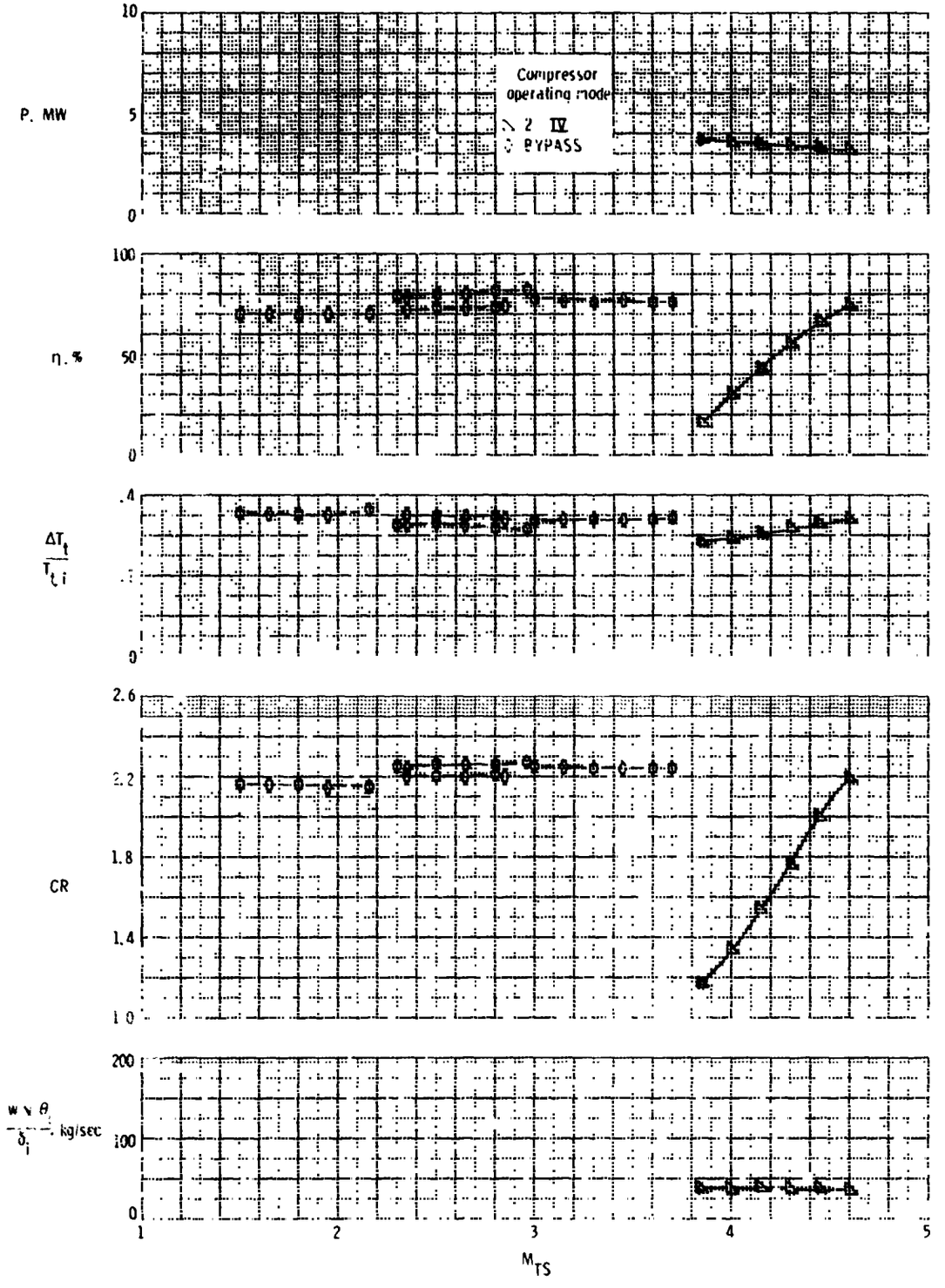

(e) Compressor G.

Figure 14.- Concluded.

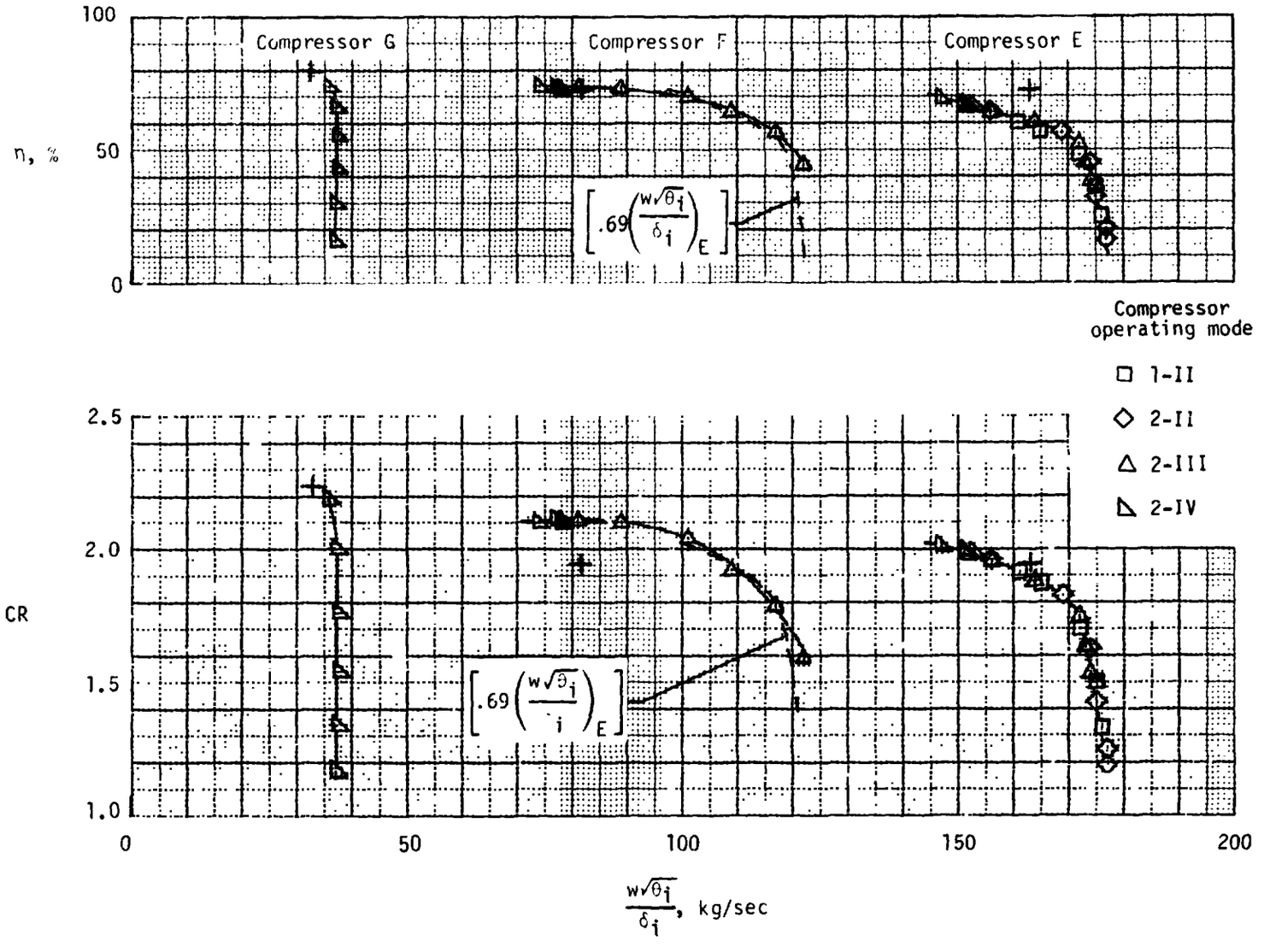

Figure 15.- Compression ratio and efficiency characteristics of compressors E, F, and G (+ denotes manufacturer's design point).

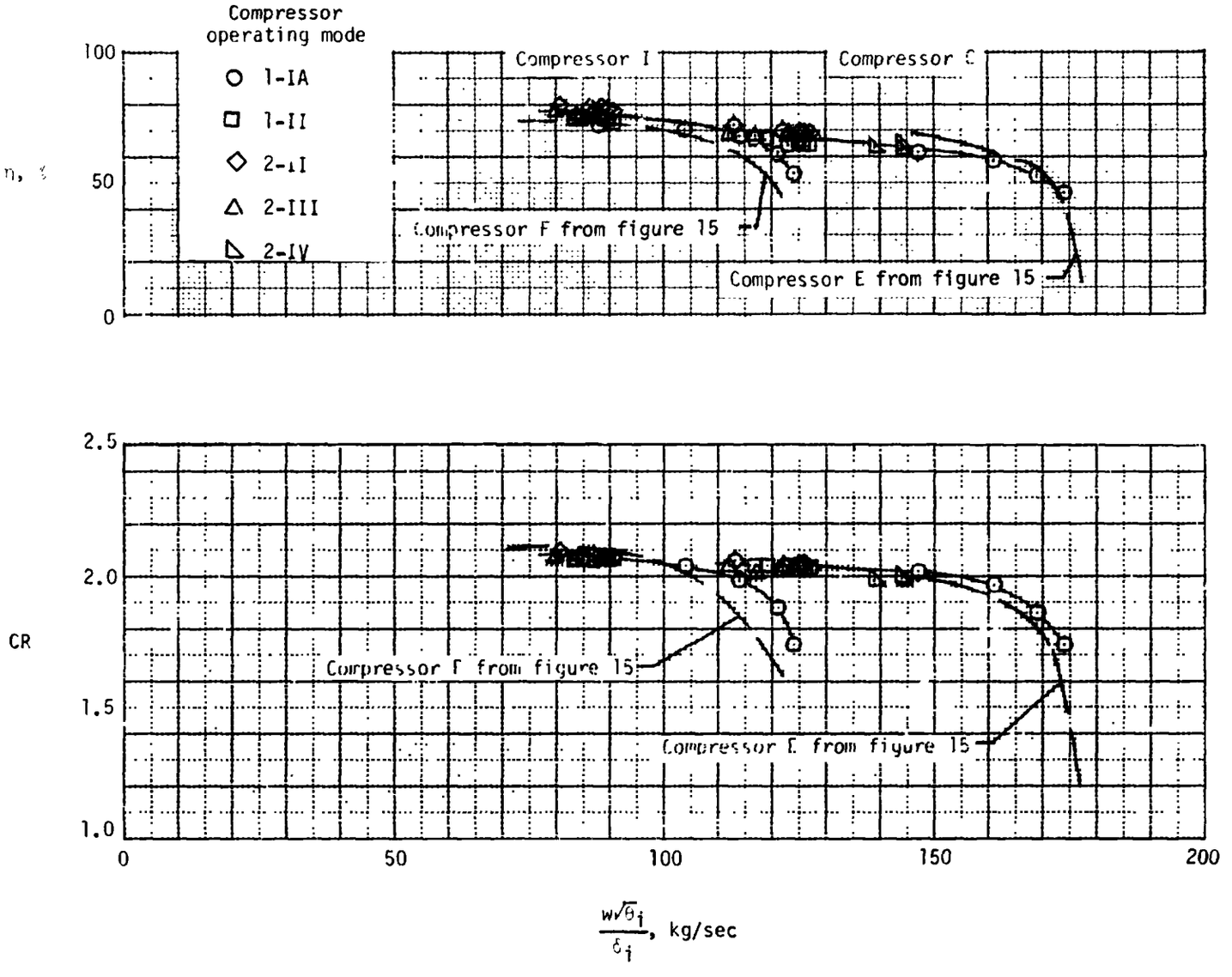

Figure 16.- Compression ratios and efficiencies of compressors I and C.

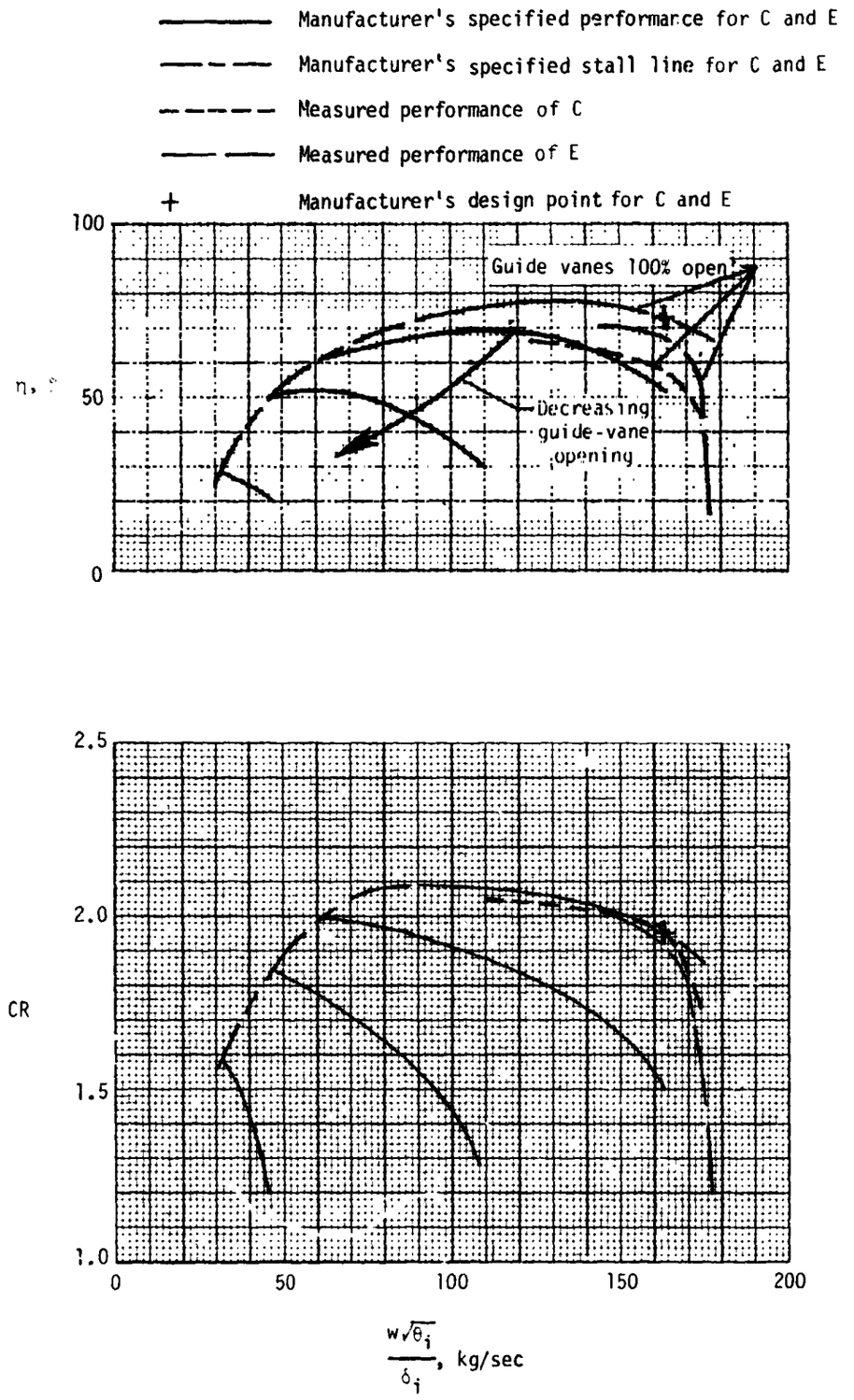

(a) Compressors C and E.

Figure 17.- Comparison of measured compressor performances with manufacturer's specifications.

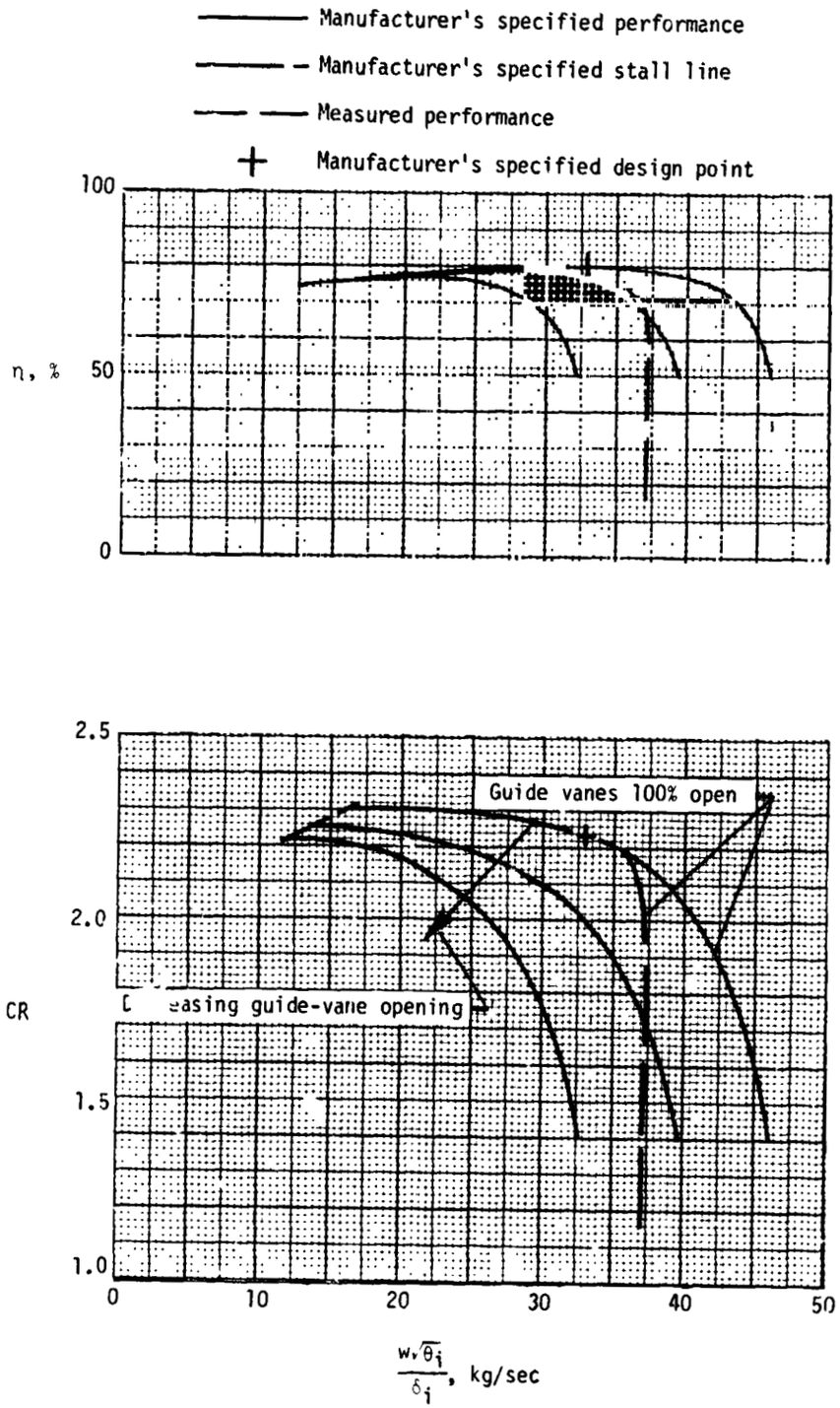

(b) Compressor C.

Figure 17.- Concluded.

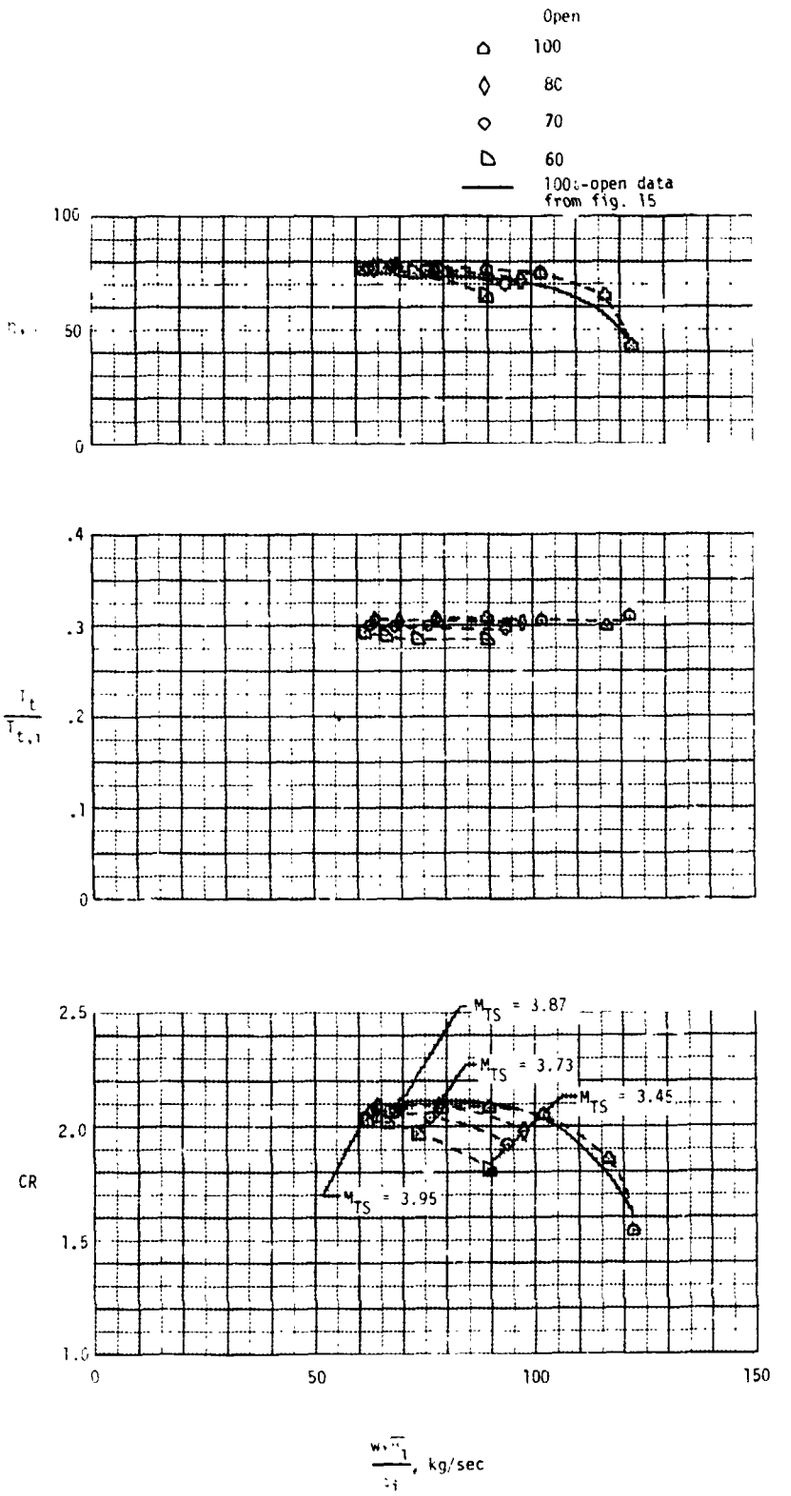

Figure 18.- Effect of inlet guide-vane position on performance of compressor F (compressor operating mode 2-III).

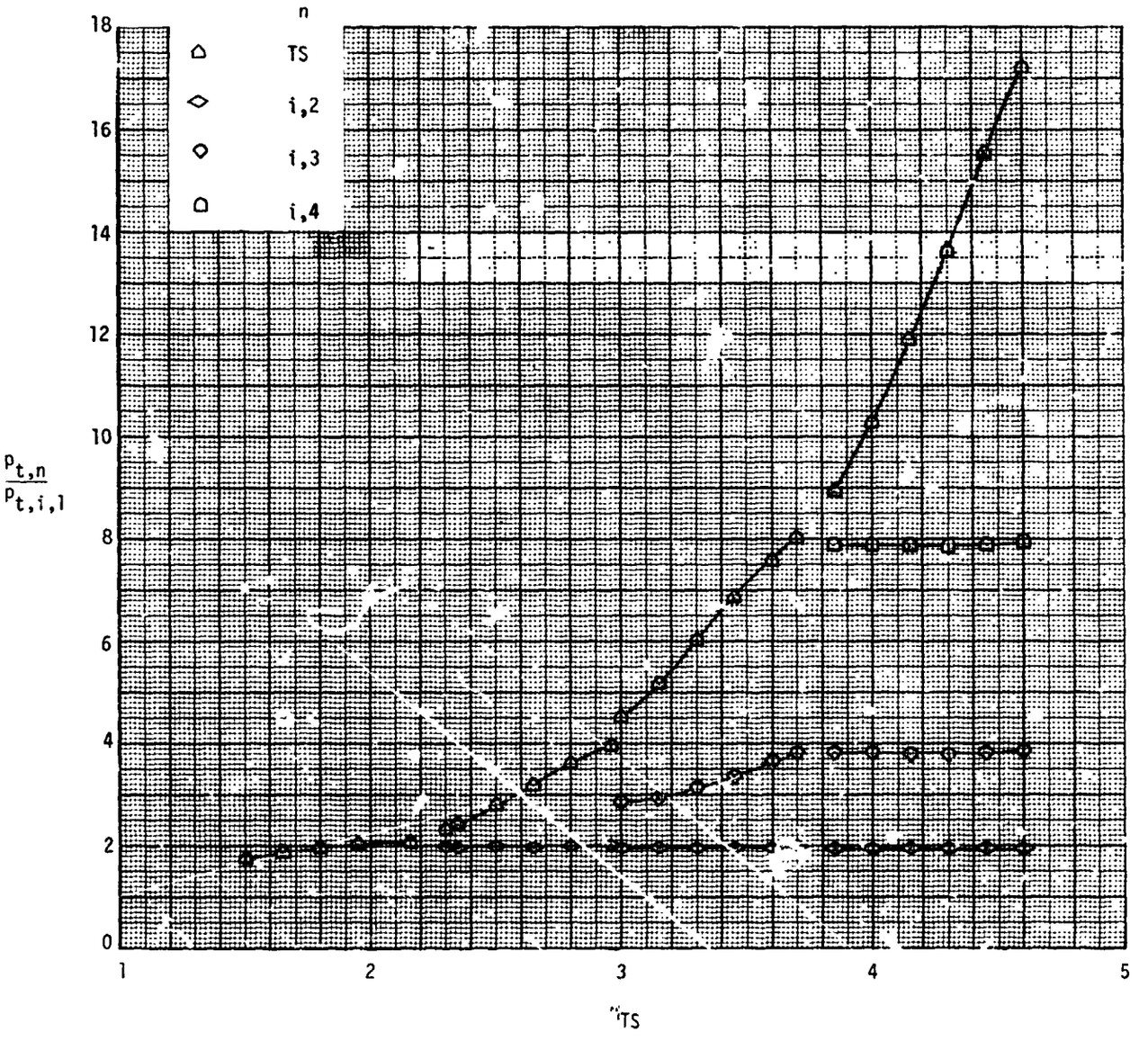

Figure 19.- Overall and incremental compression ratio performance of UPWT compressor system.

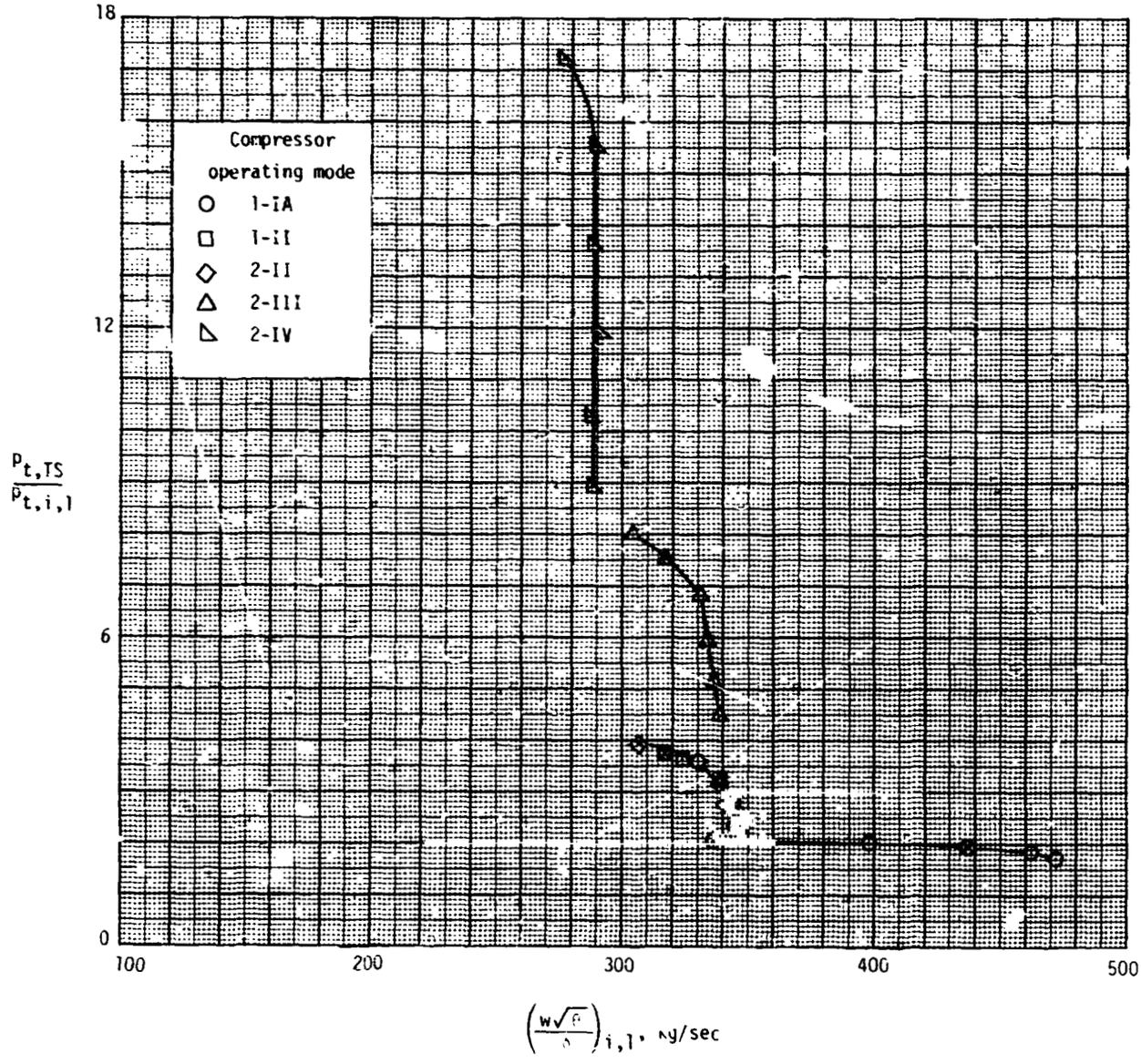

Figure 20.- Overall compression ratio performance of the compressor system.

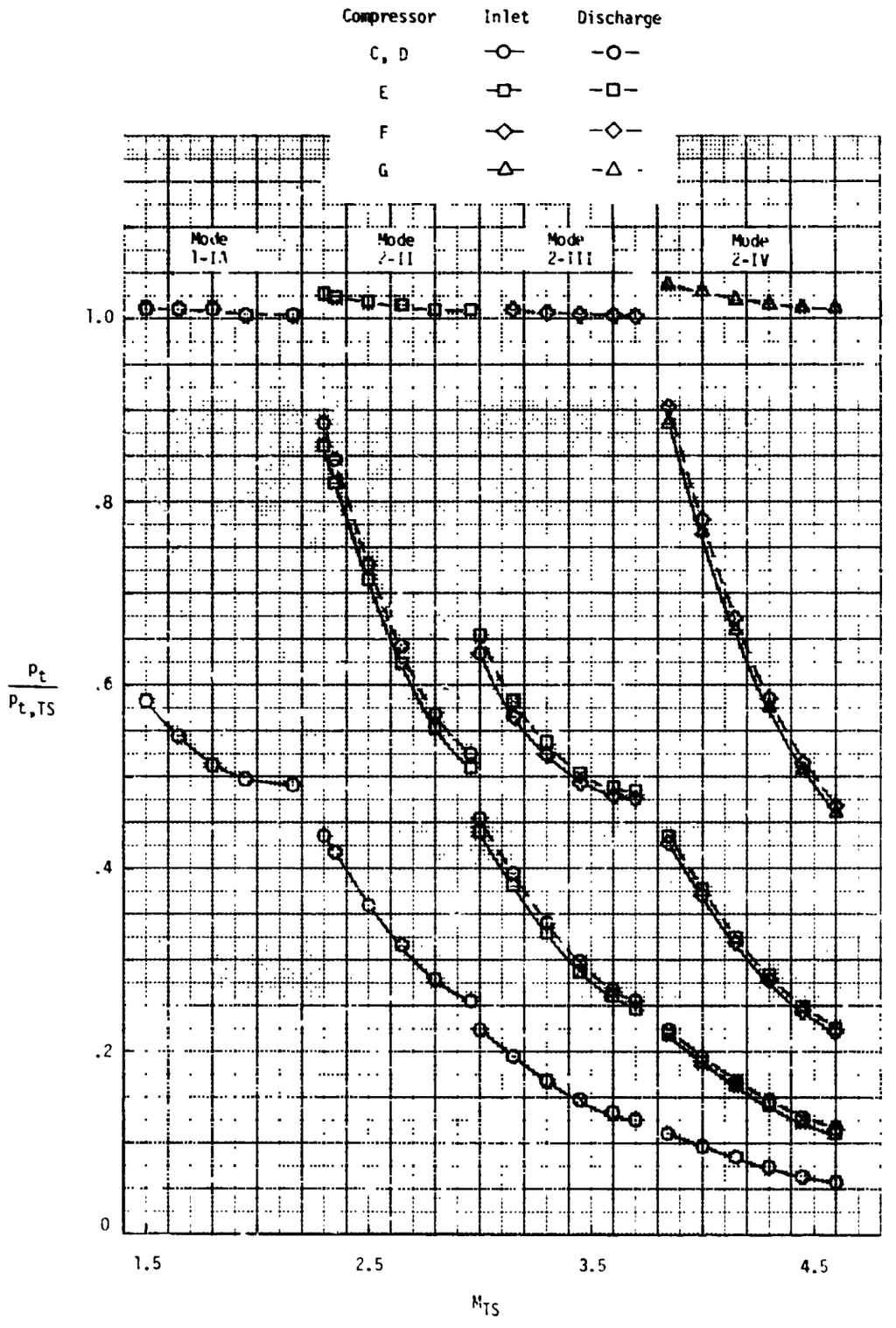

Figure 21.- Comparison of inlet and discharge pressures of compressors.

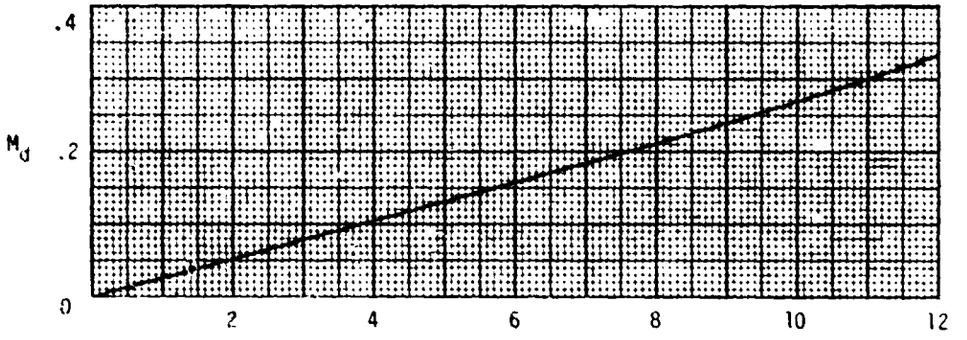

(a) Relationship between discharge Mach number and corrected duct inlet mass flow per unit area.

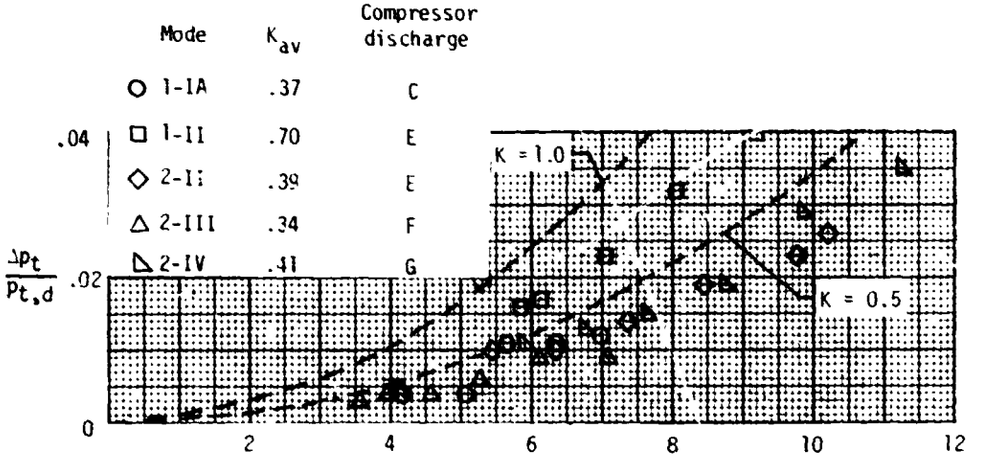

(b) Pressure losses between last stage of compression and test section.

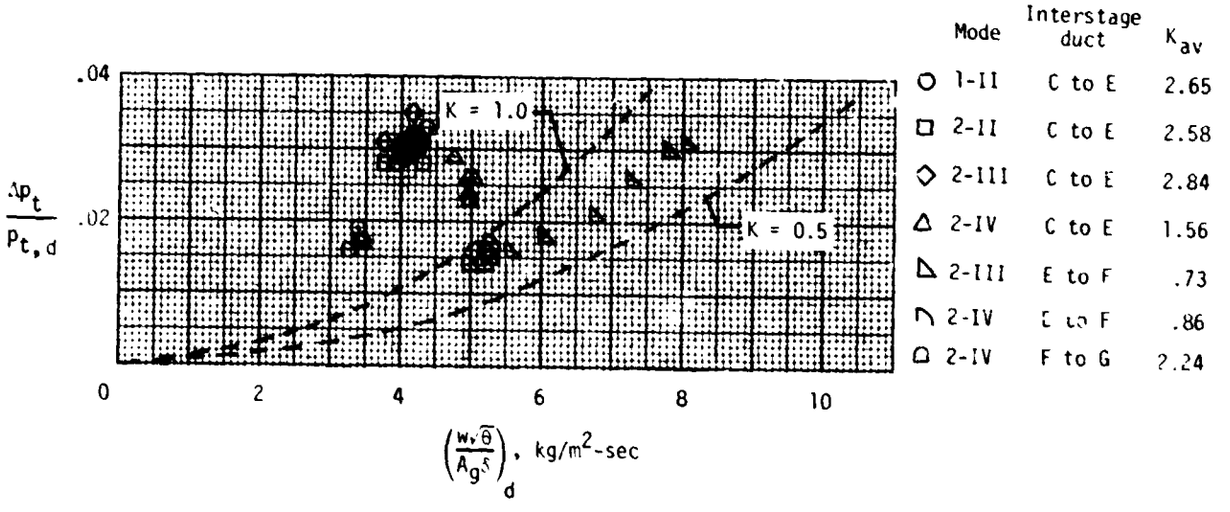

(c) Interstage pressure losses.

Figure 22.- Total presure losses in ducting downstream of compressor discharge.

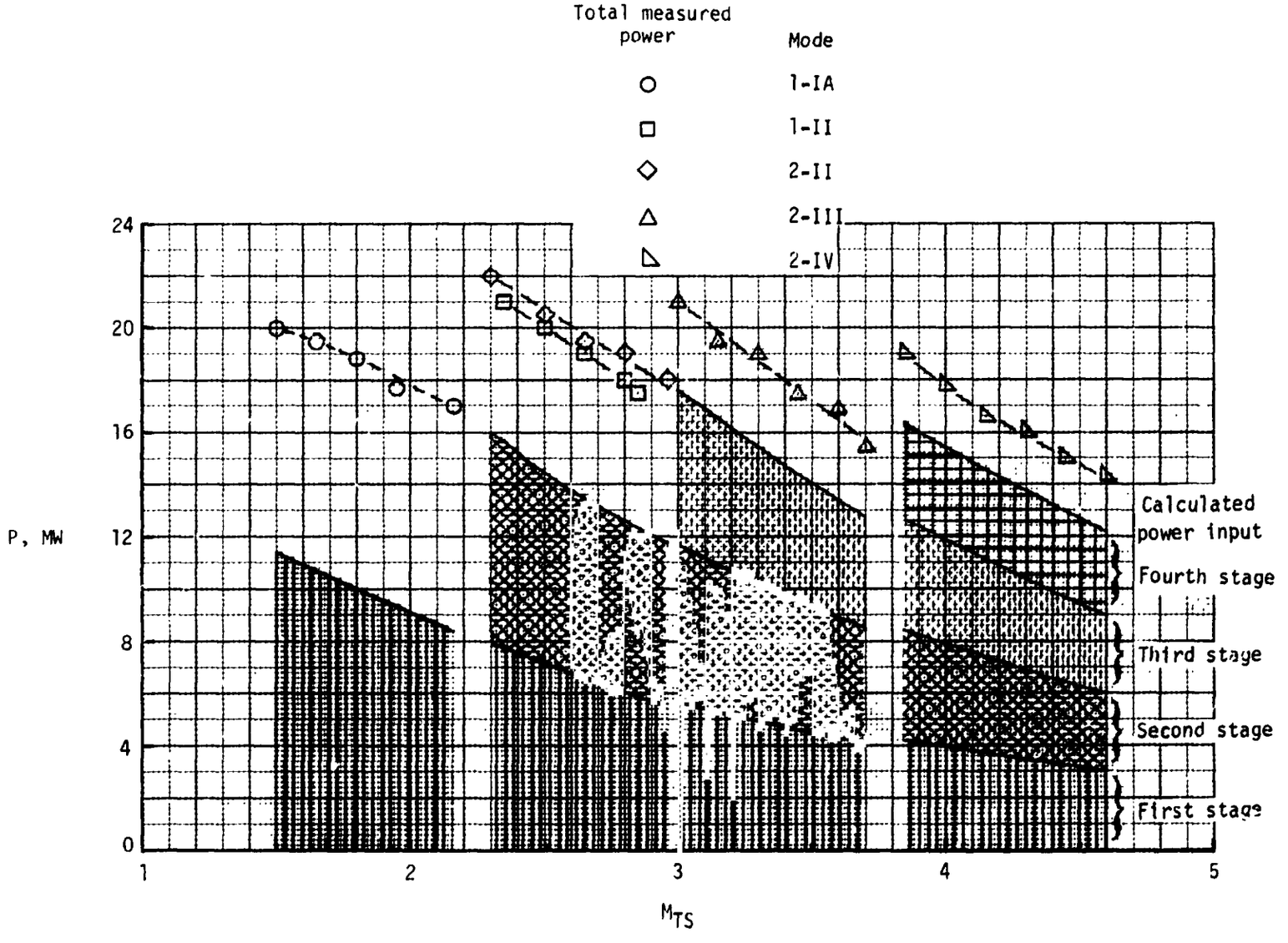

Figure 23.- Measured power input to the UPWT drive motor system. (N_{Re} = 4.92 × 10^6 per meter).

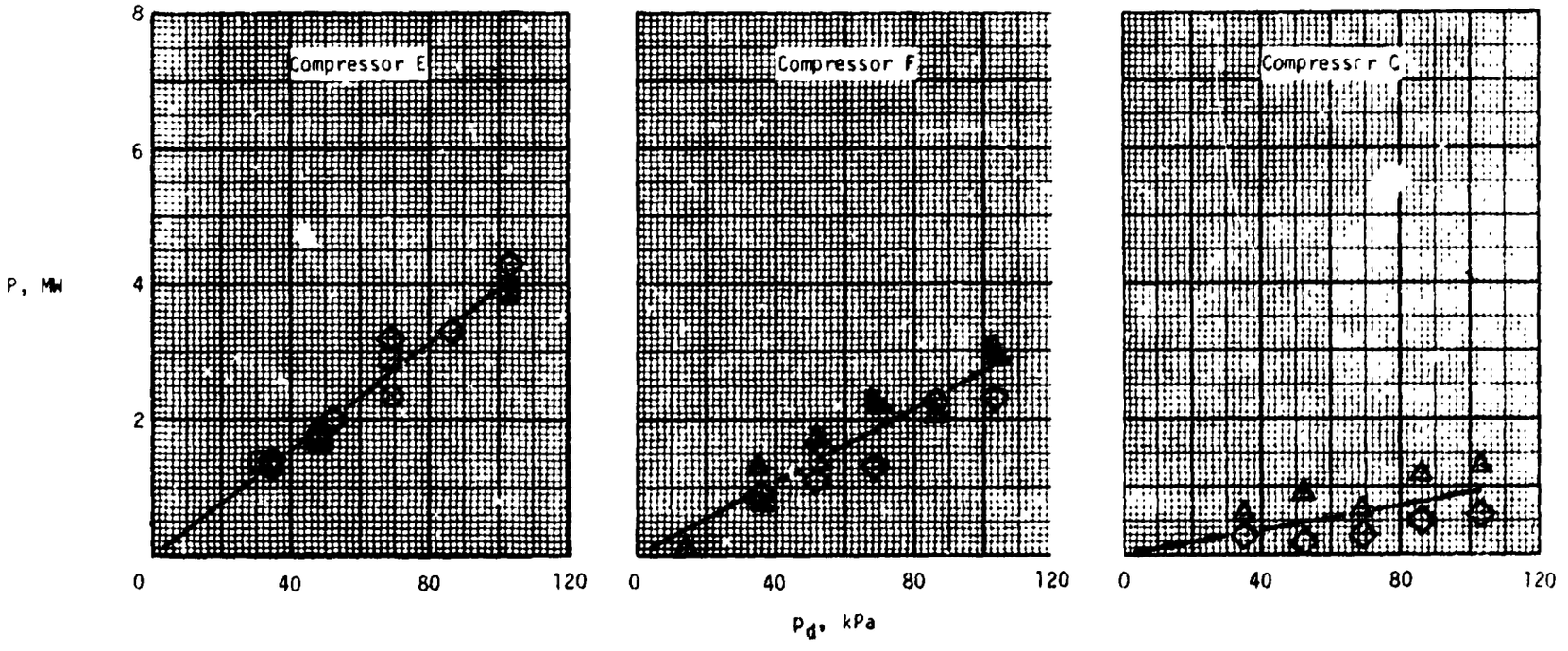

Figure 24.- Power measurements of individual compressors operating in bypass mode. Different symbols indicate repeat runs.

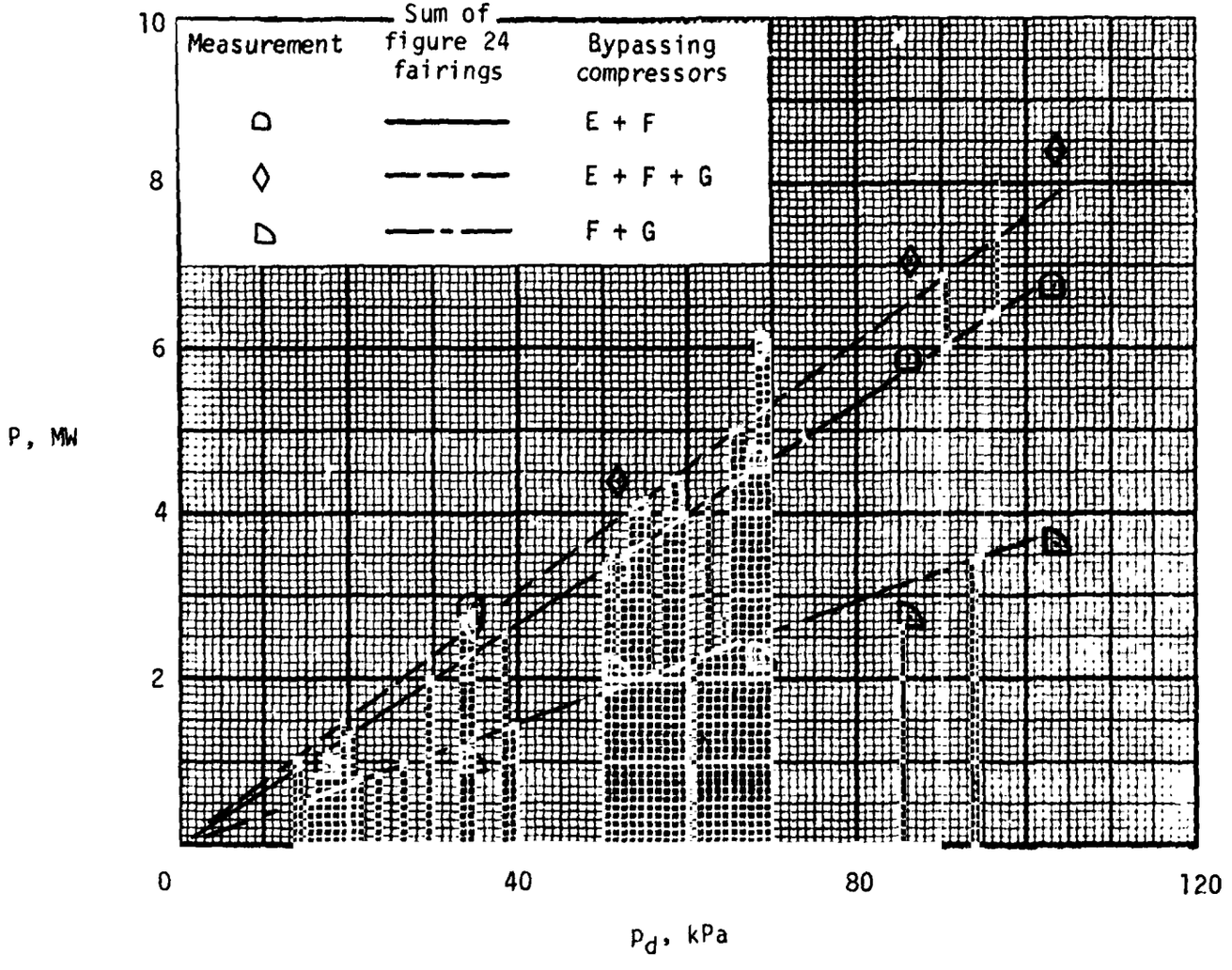

Figure 25.- Power measurements of compressor combinations operating in bypass mode.

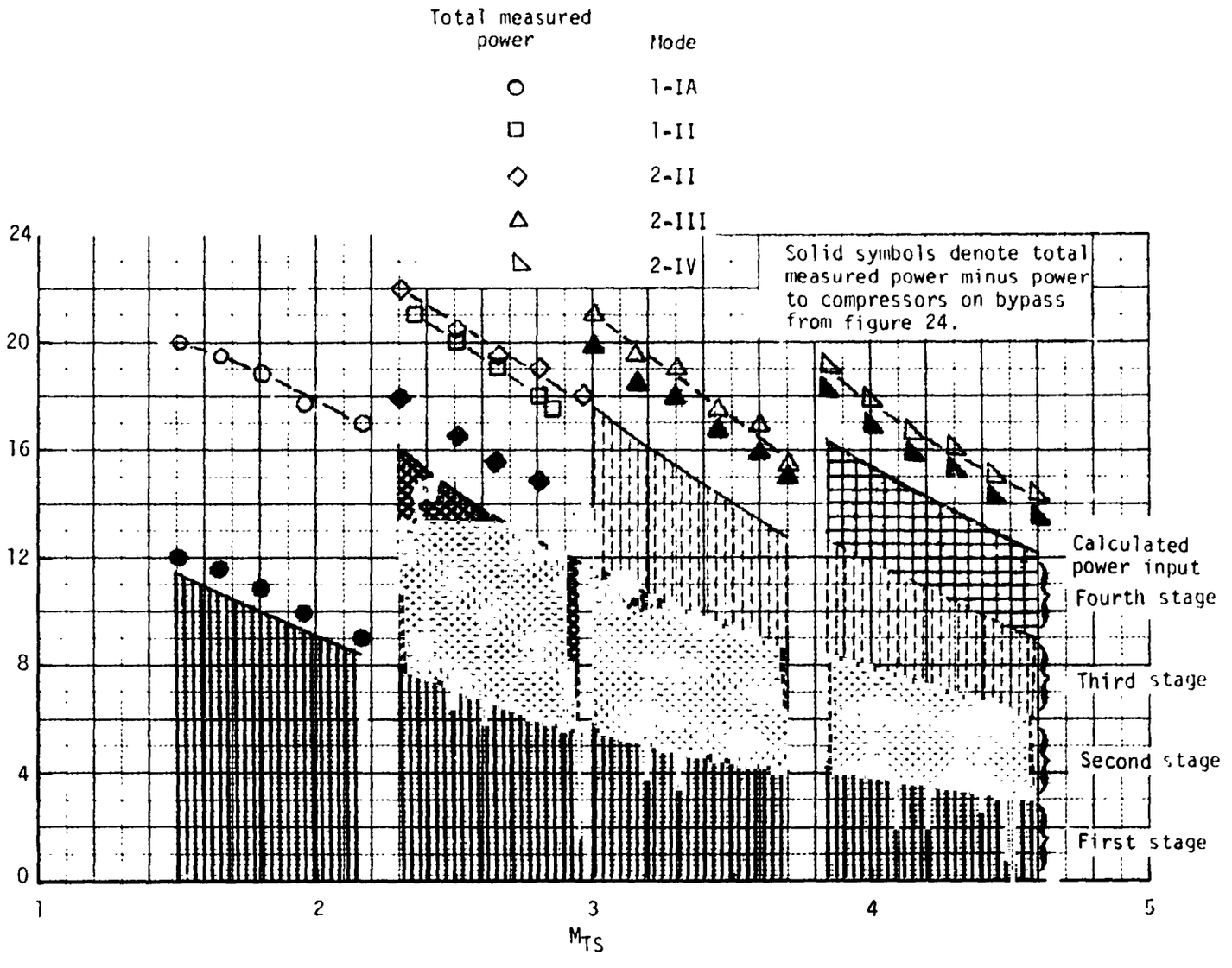

Figure 26.- Comparison of calculated power input and measured total power minus power used by compressors on bypass (N_{Re} = 4.92 × 10^6 per meter).

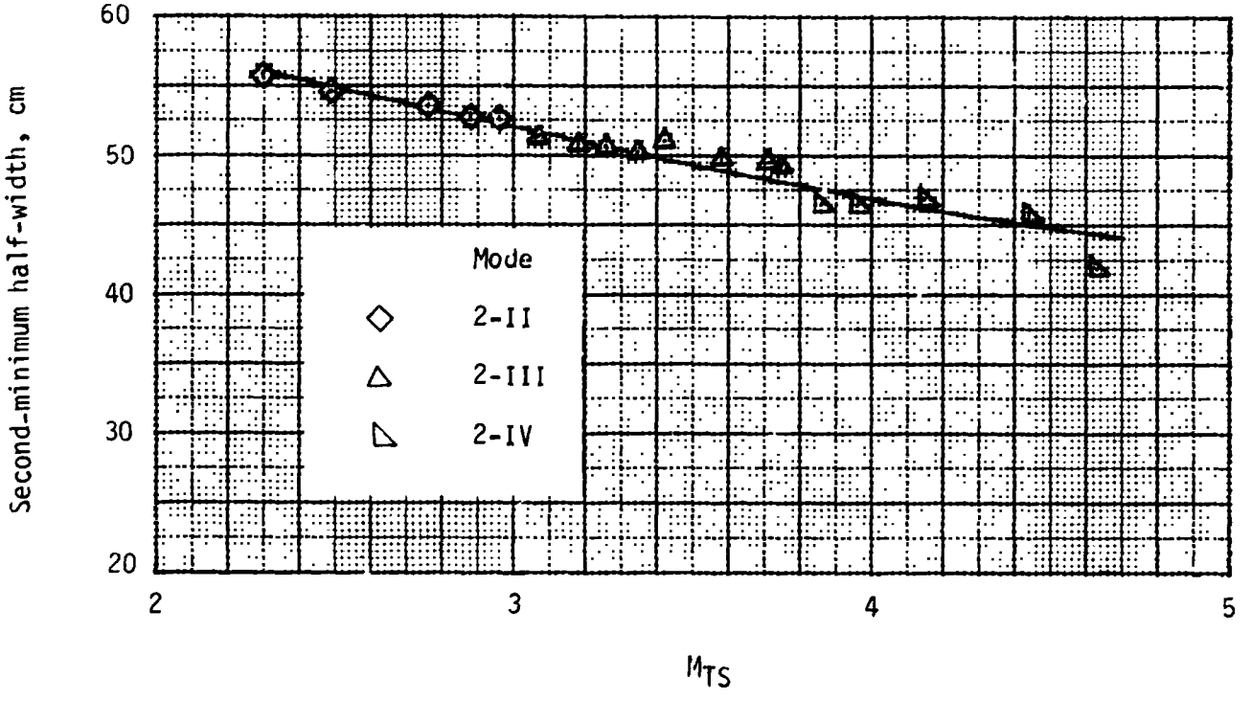

Figure 27.- Variation of operational values of second-minimum half-width with test-section Mach number (test section 2).

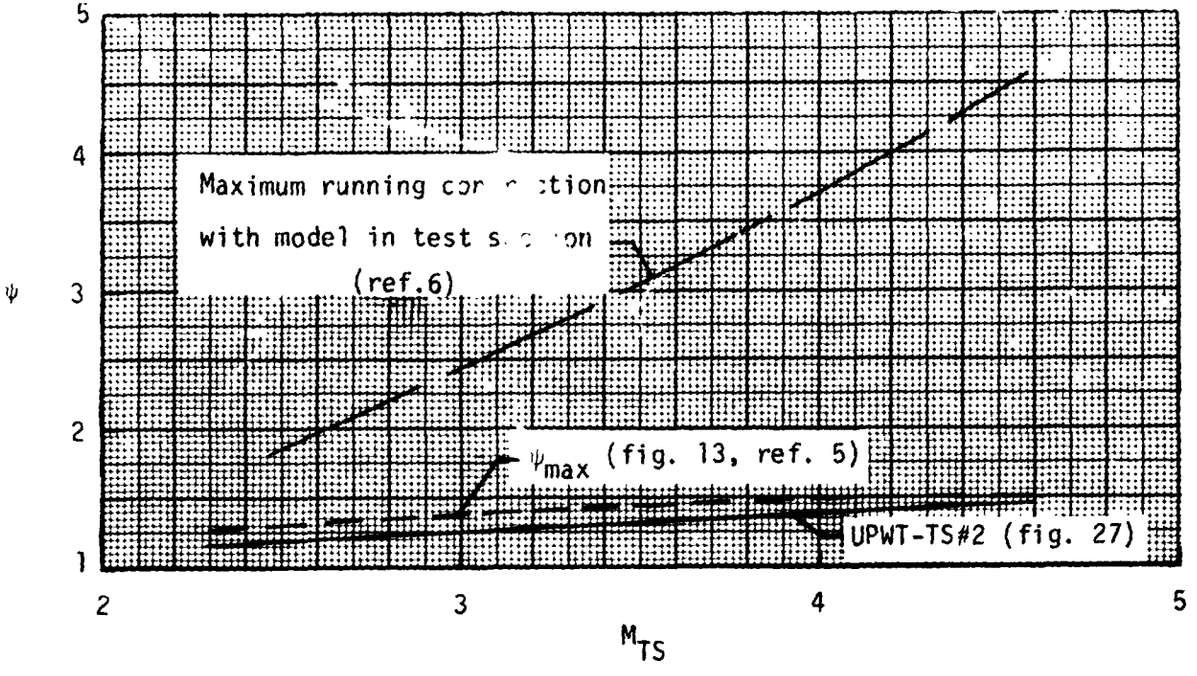

Figure 28.- Effect of Mach number on diffuser contraction ratios.

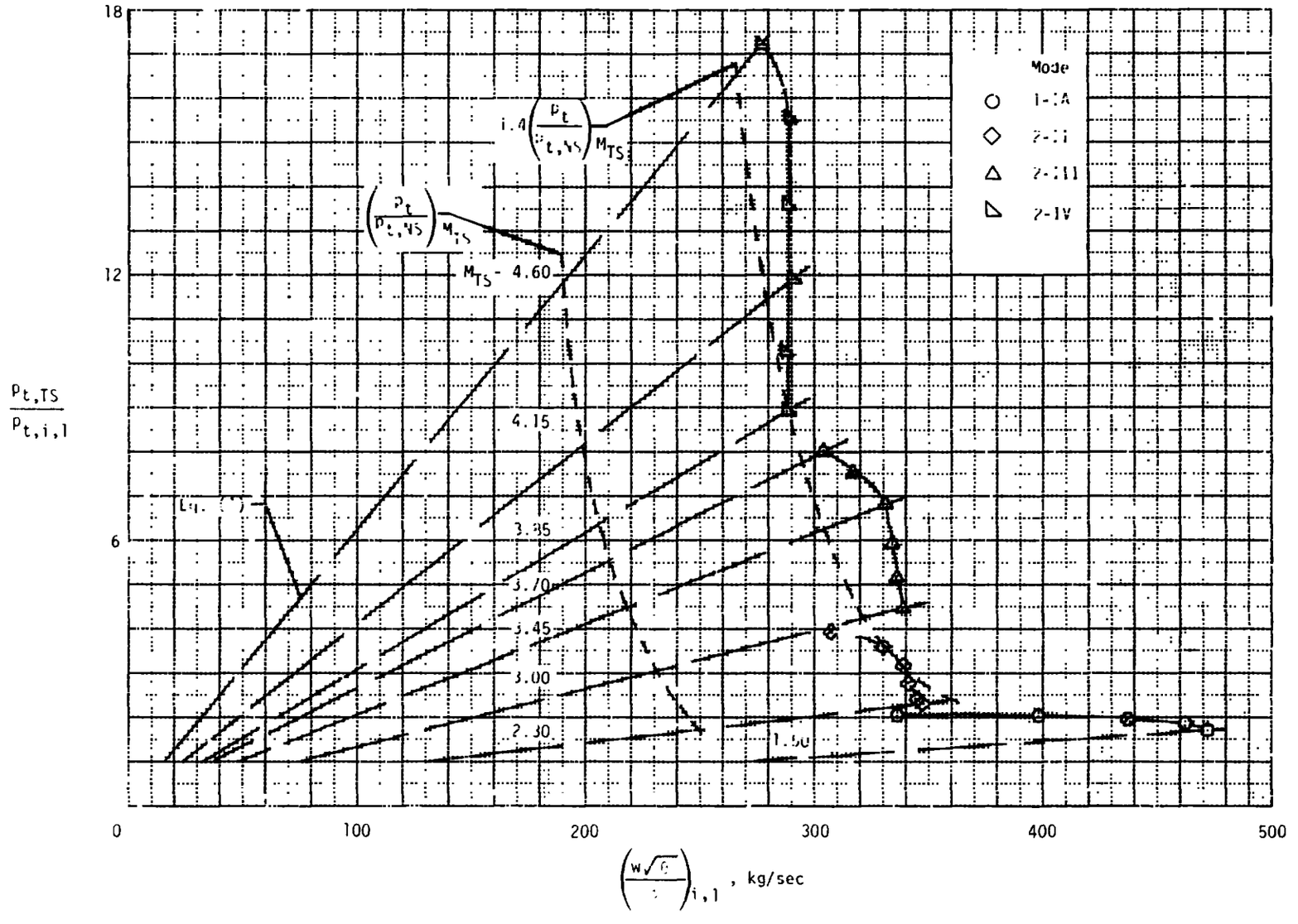

Figure 29.- Comparison of wind-tunnel and compressor characteristics of UPWT (compressor guide-vanes 100 percent open).

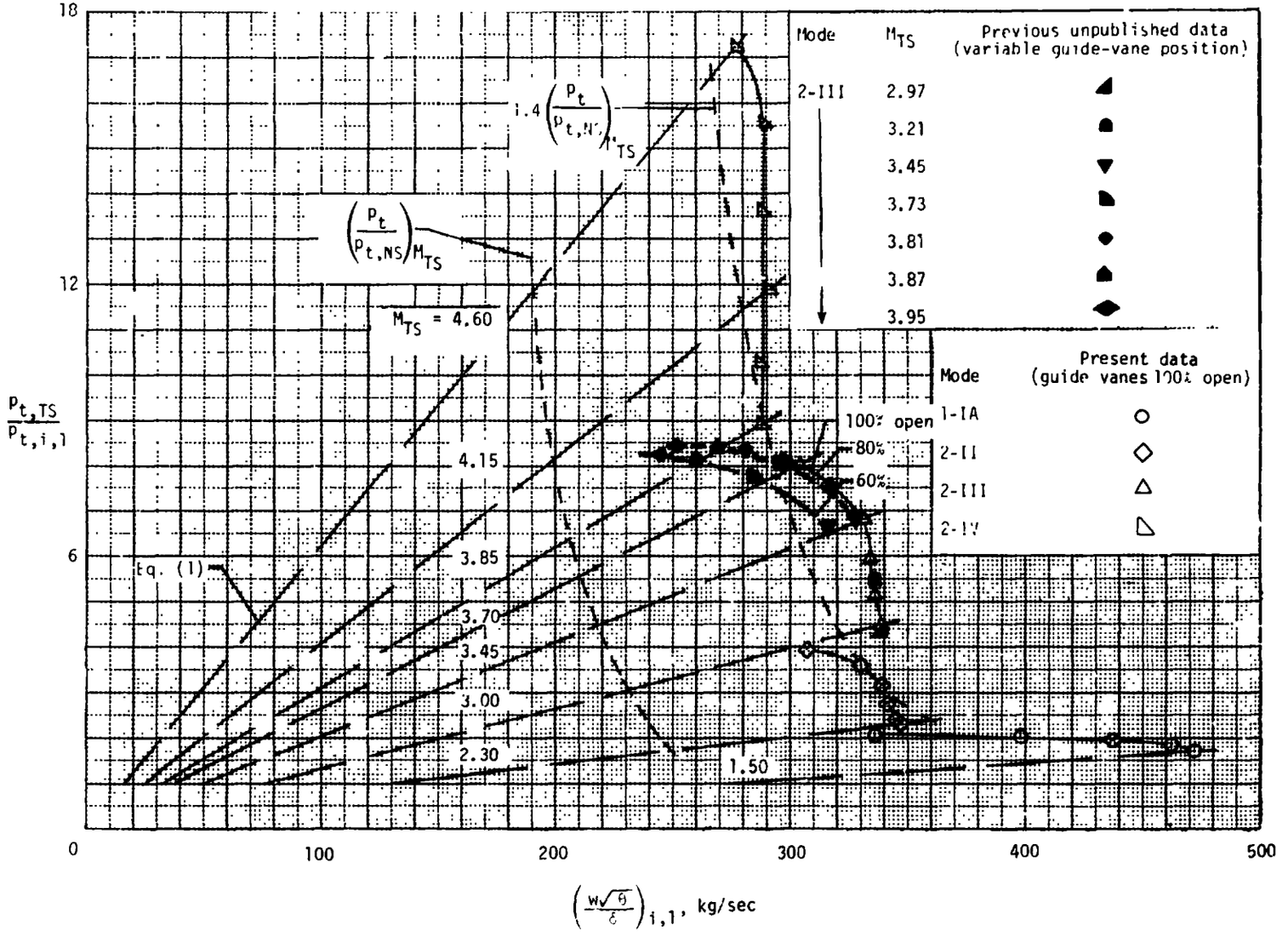

Figure 30.- Effect of guide-vane opening on matching wind-tunnel and compressor characteristics.